New Class of Supramolecular Bowl-Shaped Columnar Mesogens Derived from Thiacalix[4]arene Exhibiting Gelation and Organic Light-Emitting Diodes Applications

Vinay S.Sharma[a*], Anuj S.Sharma[b], Akshara P.Shah[c] , Priyanka A.Shah[b], Pranav S.Shrivastav[b], Mohd Athar[d]

[a]: Department of Chemistry, Faculty of Basic and Applied Sciences, Madhav University, Abu road, Sirohi, Rajasthan.*

[b]: Department of Chemistry, School of Science, Gujarat University, Ahmedabad, Gujarat.

[C]: Department of Chemistry, Mumbai University, Santacruz, Mumbai.

[d]: Department of Chemistry, Central University of Gujarat, Ghandhinagar, India.

Email address of corresponding author[a]: vinaysharma3836@gmail.com

Contents:

1. TGA, DSC data……2

2. POM data……..3

3. XRD data……...4

4. UV, fluorescence data…….....5

5. CV data…… ….....6-7

6. Optimized structures, HOMO-LUMO……8-11

7. Gelation data…….....11-16

8. Electroluminescence data……..17-18

8. ^{1}H NMR, ^{13}C NMR and ESI-Mass……...…….....19-42

9. References……....43

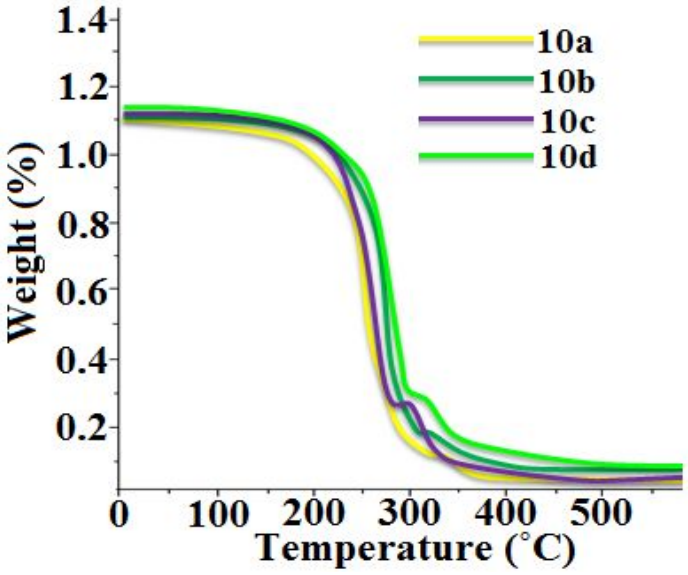

Figure S1. TGA curves of the compounds **10a-10d** carried out at a rate of 10˚C/min.

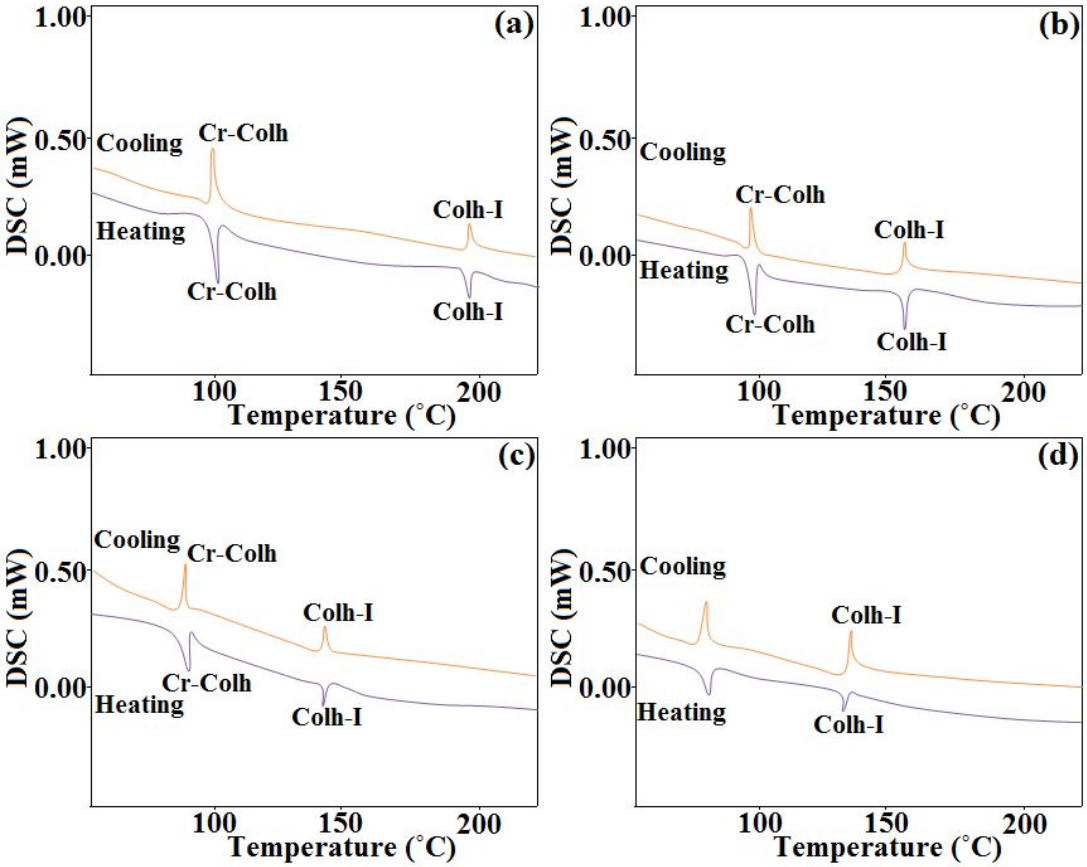

Figure S2. The DSC traces of compounds **10a** (a), **10b** (b), **10c** (c) and **10d** (d) on first heating and cooling (scan rate 10˚C/min).

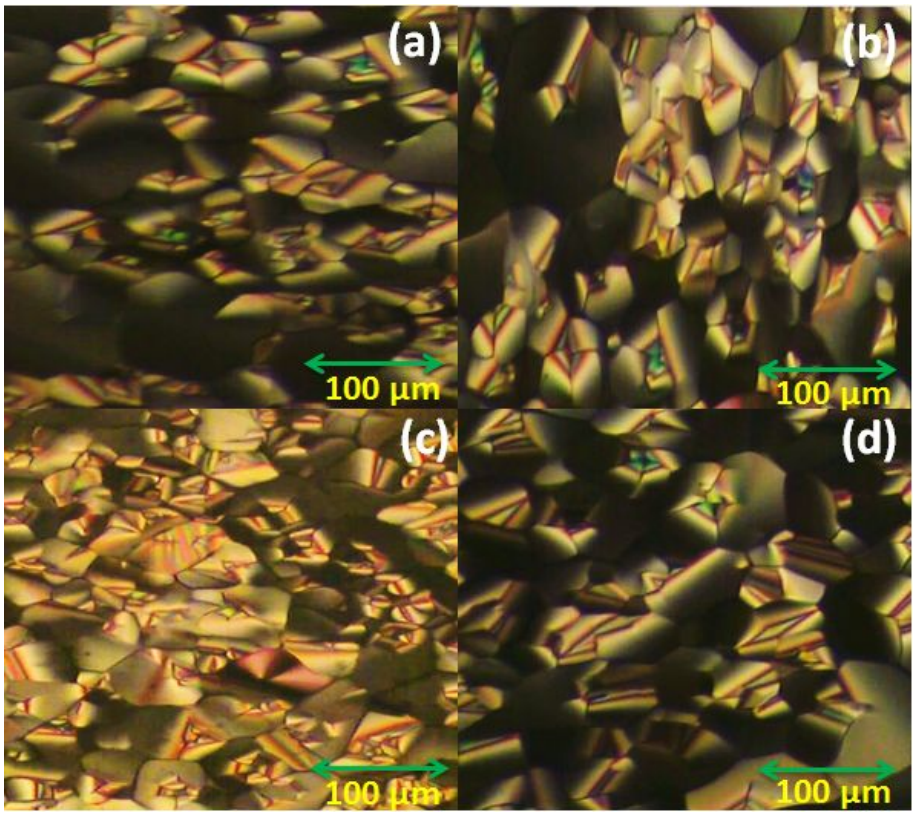

Figure S3. POM texture image of compound **10a** at 102.8 ˚C (a) compound **10b** at 94.8 ˚C (b) compound **10c** at 75.2 ˚C (c) and compound **10d** at 61.6 ˚C (d) on heating condition from solid crystalline state as seen under cross polarizers.

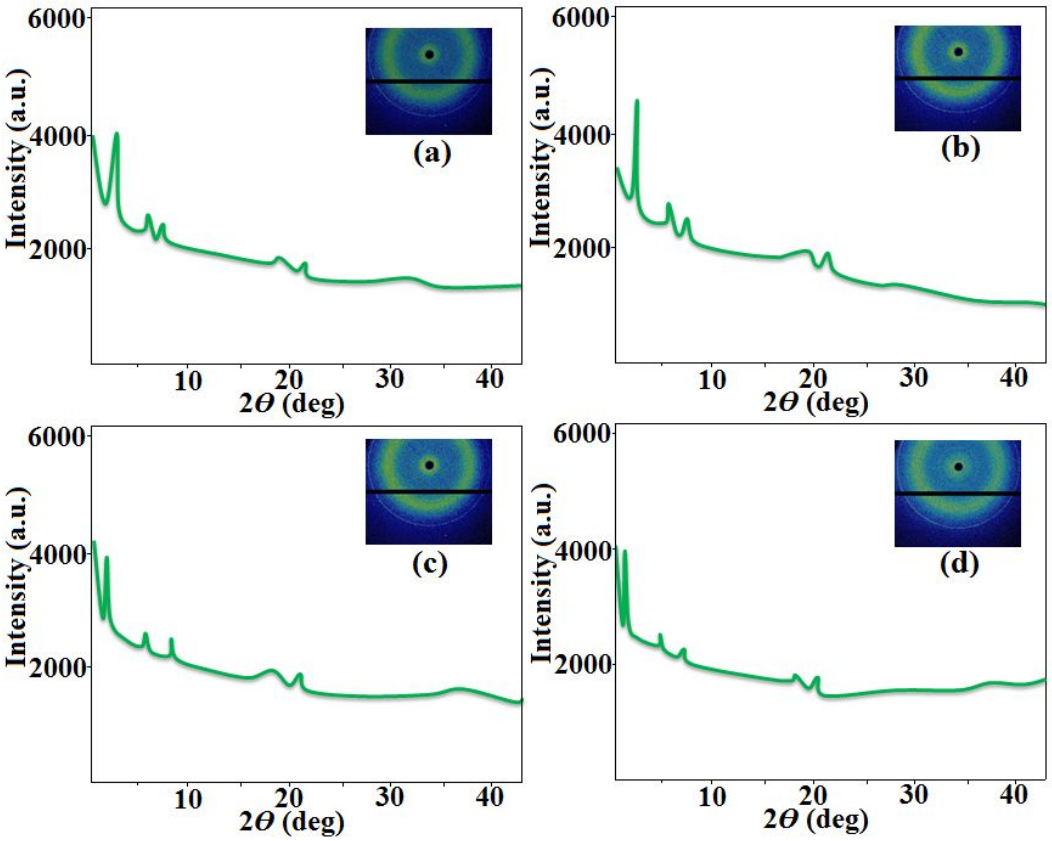

Figure S4. XRD profiles depicting the intensity against the 2Θ obtained for the Col_h phase of compound **10a** at 104.0 ˚C (a); Col_h phase of compound **10b** at 94.0 ˚C (b); Col_h phase of compound **10c** at 78.0 ˚C (c); Col_h phase of compound **10d** at 66.0˚C (d) on cooling from isotropic temperature; the insert shows the image pattern obtained.

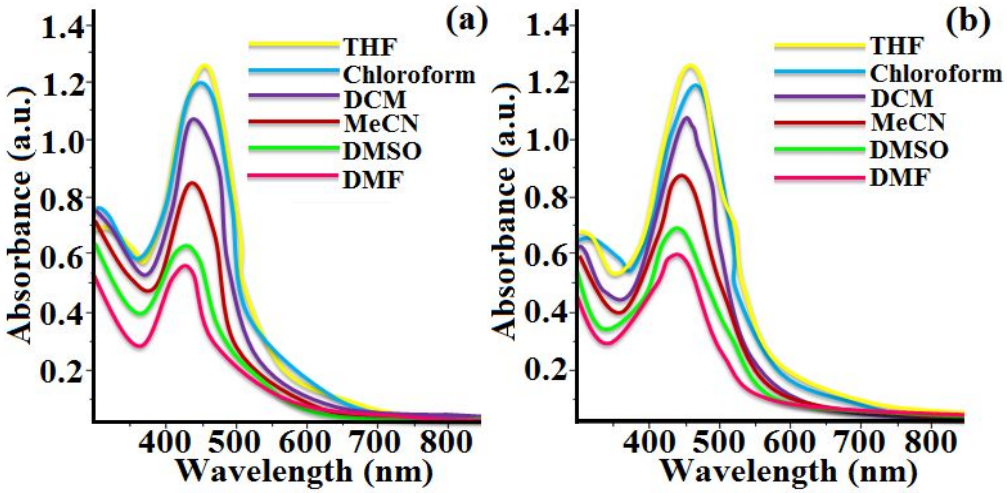

Figure S5. Absorption spectra of compound **10a** (a); compound **10d** (b) in different solvents (0.05 μM).

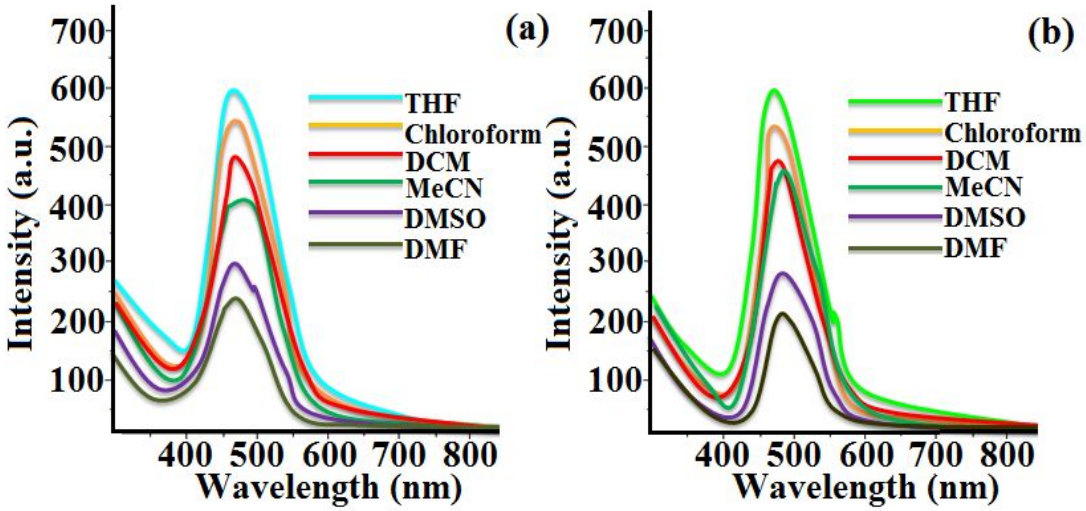

Figure S6. Fluorescence spectra of compound **10a** (a); compound **10d** (b) in different solvents (0.05 μM).

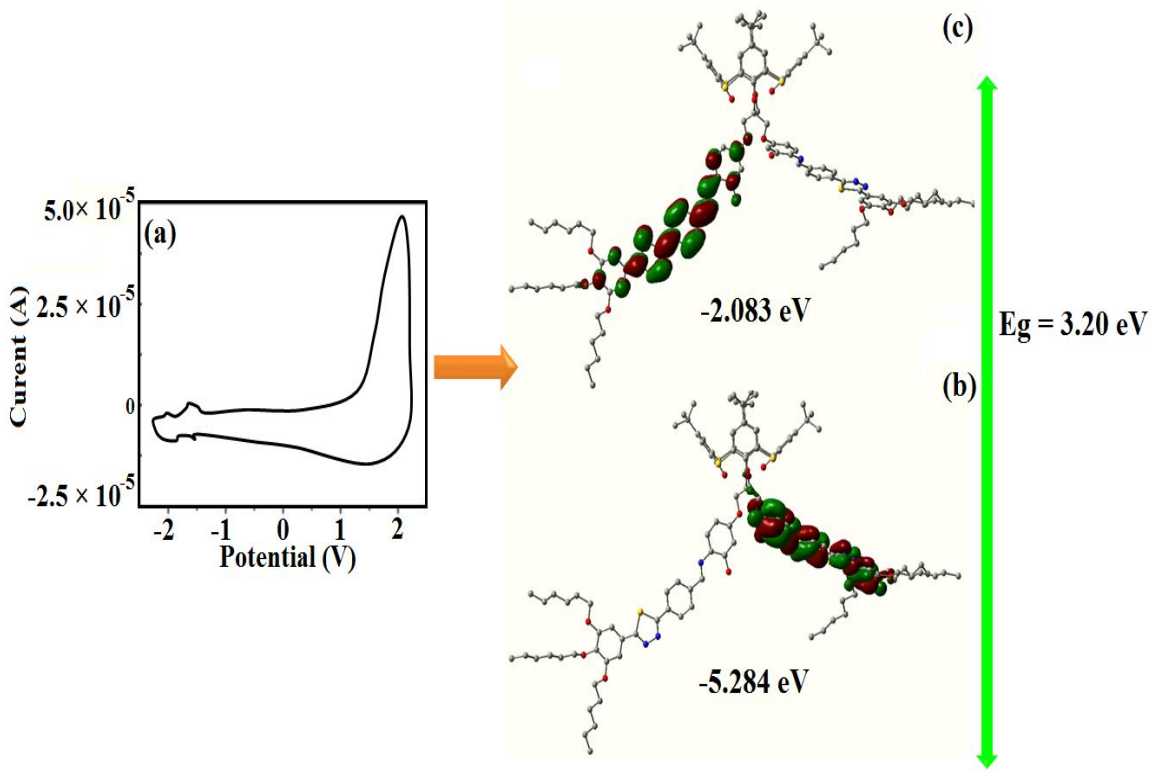

Figure S7. (a) Cyclic voltammogram of compound **10b** in anhydrous THF solution of TBAP (0.1 M) at a scanning rate of 0.5 mV/s. (b,c) The HOMO and LUMO levels of compound **10b** obtained from DFT calculation at the B3LYP/3-21G*level using Gaussian 09. Hydrogen atoms were omitted for clarity.

Table S_1. Electrochemical properties of compounds **10a-10d**

Comp.	Eoxd	Ered	E_{HOMO}	E_{LUMO}	ΔE_g, CV
10a	1.59	-1.52	-5.82	-2.71	3.11
10b	1.57	-1.50	-5.80	-2.72	3.08
10c	1.58	-1.49	-5.81	-2.74	3.07
10d	1.61	-1.54	-5.85	-2.69	3.16

Experimental conditions: Ag/AgNO3 as a reference electrode, platinum wire as counter electrode, glassy carbon as working electrode, tetrabutylammonium perchlorate (0.1 M) as supporting electrolyte, room temperature

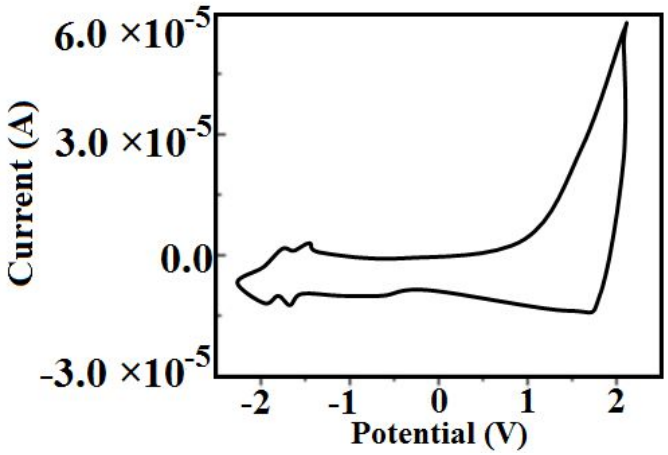

Figure S8. Cyclic voltammogram of compound **10c** in anhydrous THF solution of TBAP (0.1 M) at a scanning rate of 0.5 mV/s.

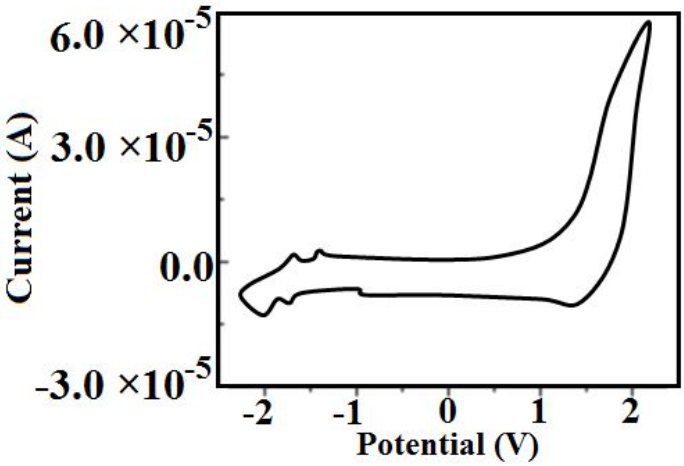

Figure S9. Cyclic voltammogram of compound **10d** in anhydrous THF solution of TBAP (0.1 M) at a scanning rate of 0.5 mV/s.

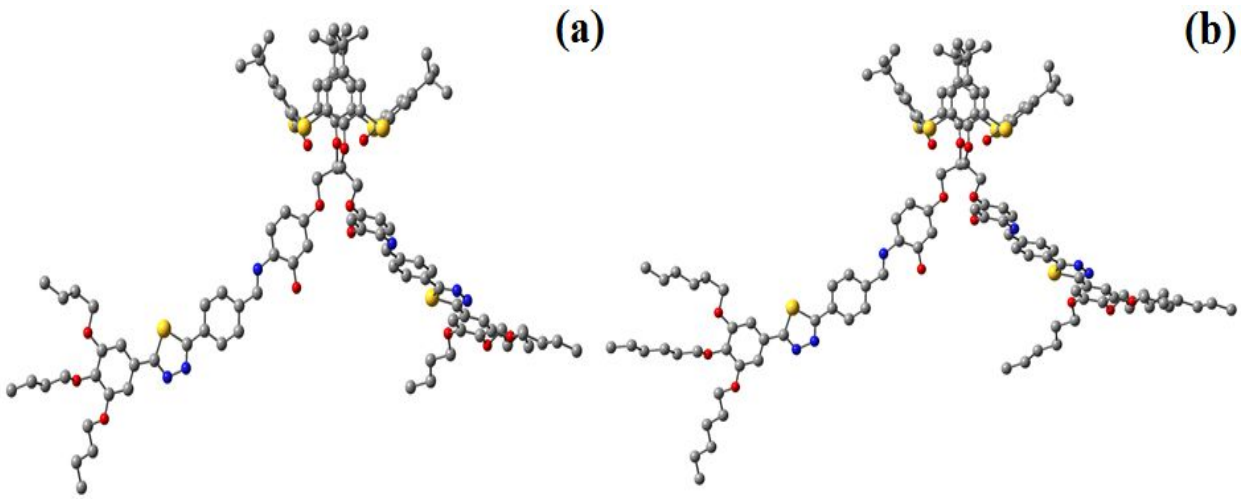

Figure S10. Optimized geometries of 1,3,4-thiadiazole based thiacalix[4]arene derivatives (a) **10a** (cone conformation); (b) **10b** (cone conformation) at B3LYP/3-21G level. Hydrogens were omitted for clarity.

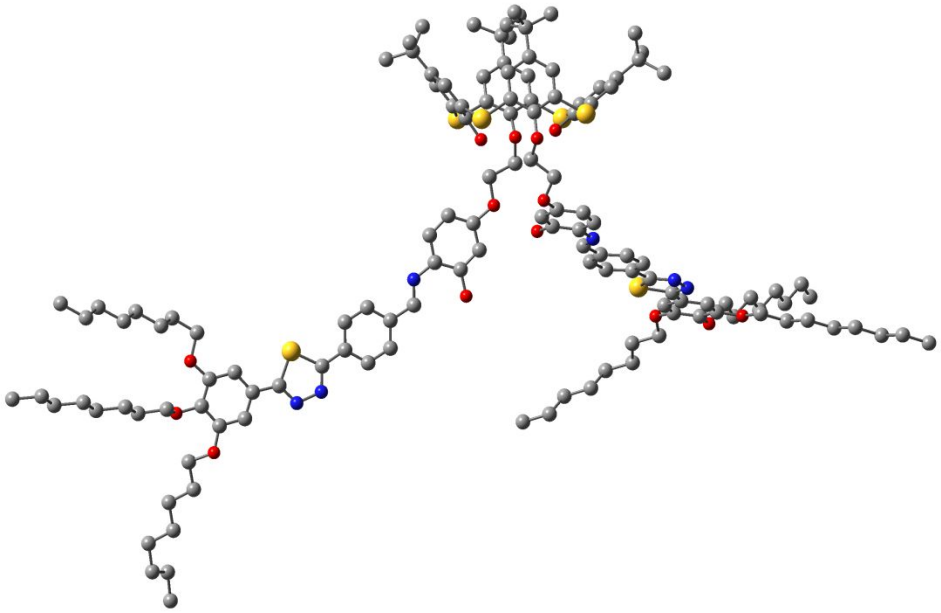

Figure S11. Optimized geometries of 1,3,4-thiadiazole based thiacalix[4]arene derivatives **10c** (cone conformation) at B3LYP/3-21G level. Hydrogens were omitted for clarity.

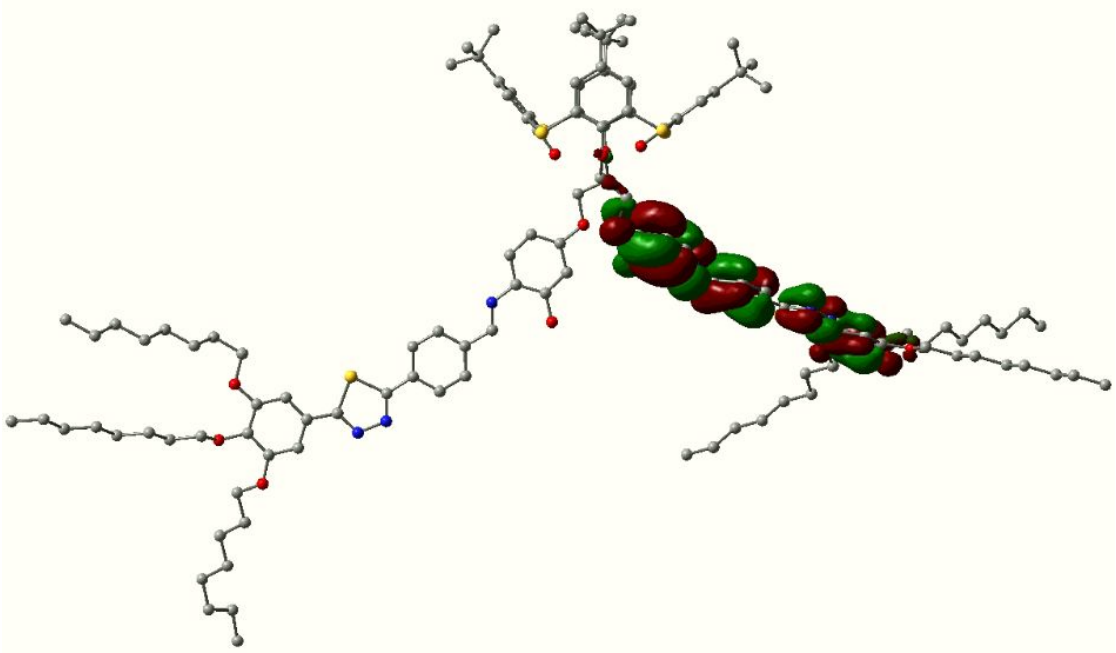

Figure S12. The HOMO energy levels of compound **10c** obtained from DFT calculation at the B3LYP/3-21G* level. Hydrogen atoms were omitted for clarity.

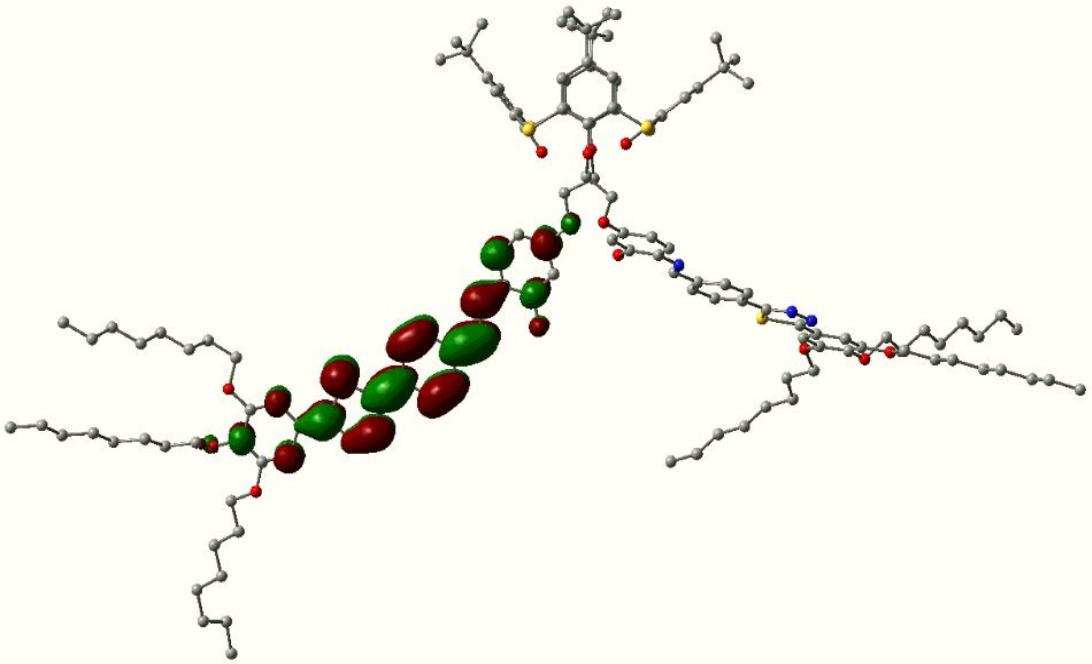

Figure S13. The LUMO energy levels of compound **10c** obtained from DFT calculation at the B3LYP/3-21G* level. Hydrogen atoms were omitted for clarity.

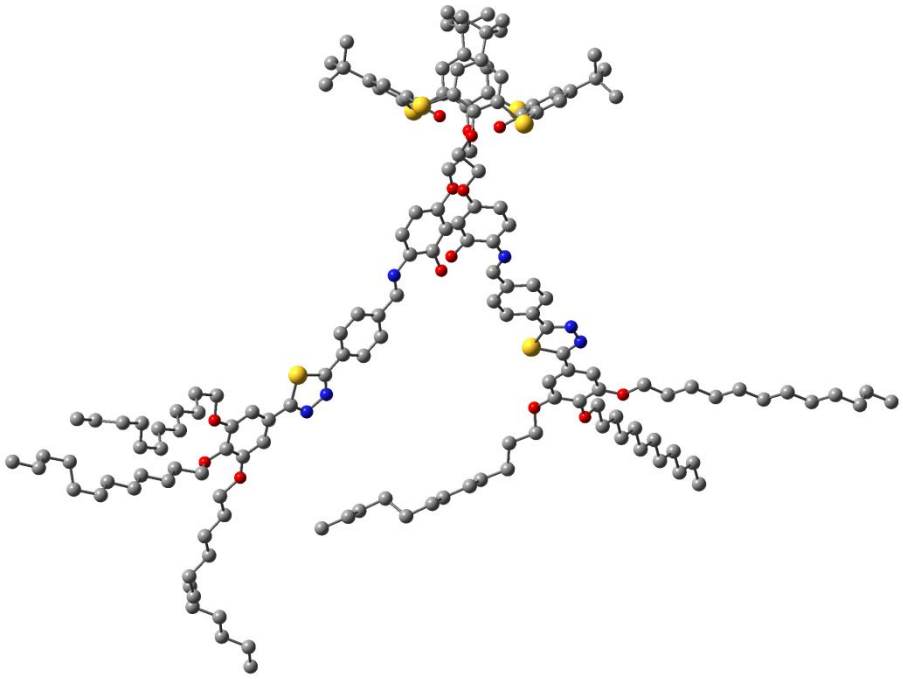

Figure S14. Optimized geometries of 1,3,4-thiadiazole based thiacalix[4]arene derivatives **10d** (cone conformation) at B3LYP/3-21G level. Hydrogens were omitted for clarity.

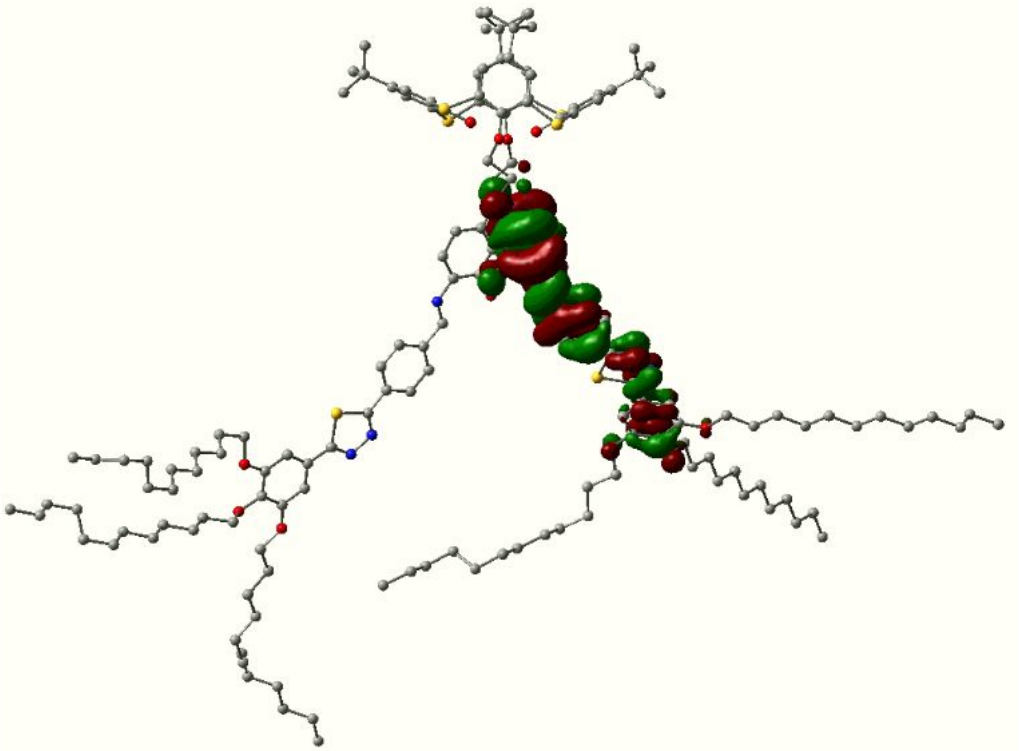

Figure S15. The HOMO energy levels of compound **10d** obtained from DFT calculation at the B3LYP/3-21G* level. Hydrogen atoms were omitted for clarity.

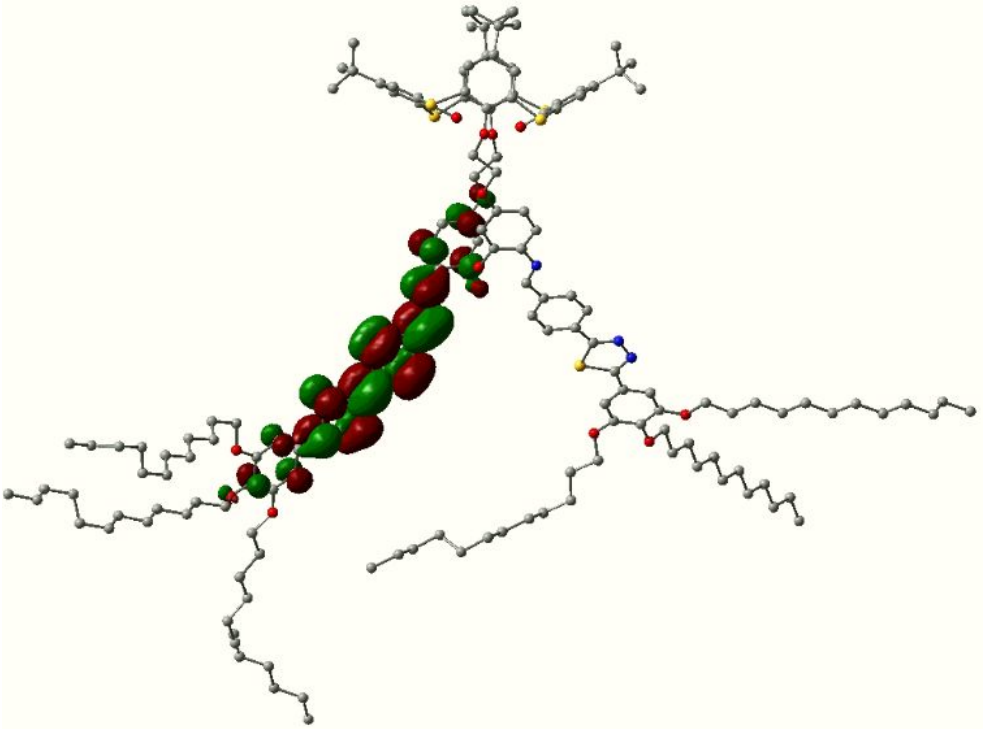

Figure S16. The LUMO energy levels of compound **10d** obtained from DFT calculation at the B3LYP/3-21G* level. Hydrogen atoms were omitted for clarity.

Table S_2. Gelation behaviour of compound **10c** and **10d**

Sr.No.	**Solvent**	**Comp.10c**		**Comp.10d**	
		Properties	**CGC (wt %)**	**Properties**	**CGC (wt %)**
1	Decane	G(O)	1.6 wt %	G(O)	1.9 wt %
2	Dodecane	G(O)	1.1 wt %	G(O)	1.5 wt %
3	Toluene	S	-	S	-
4	Benzene	S	-	S	-
5	DCM	S	-	S	-

6	THF	S	-	S	-
7	Chloroform	S	-	S	-
8	Ethanol	P	-	P	-
9	Butanol	P	-	P	-
10	Methanol	P	-	P	-

G = stable gel; P = precipitate; O = opaque; S = the critical gelation concentration (wt %) is the minimum concentration necessary for gelation.

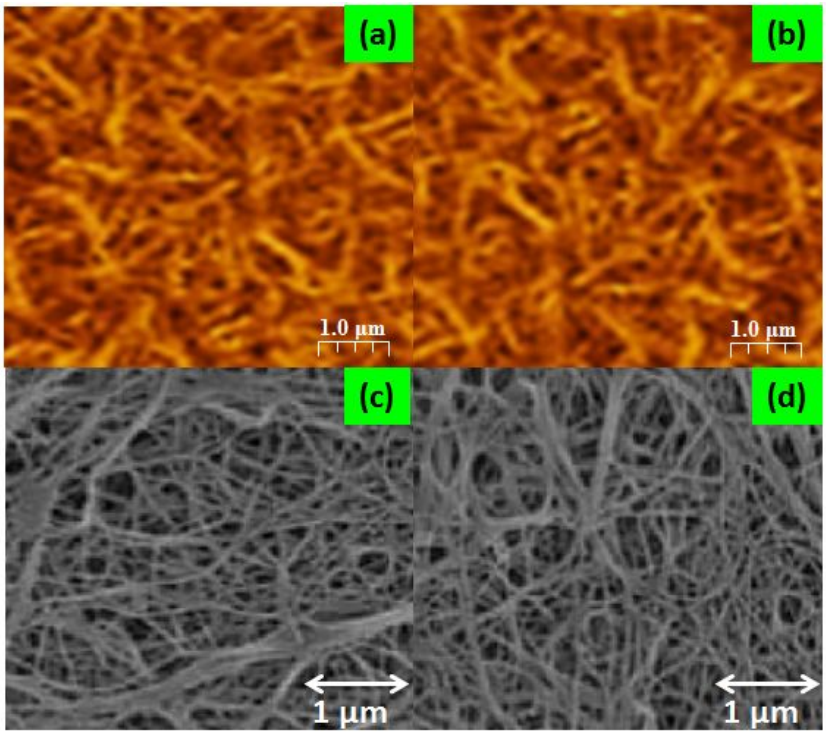

Figure S17. AFM and SEM images obtained for compound **10c** (a,c); compound **10d** (b,d) at 1mM in the dodecane solution (scale bar is 1µm).

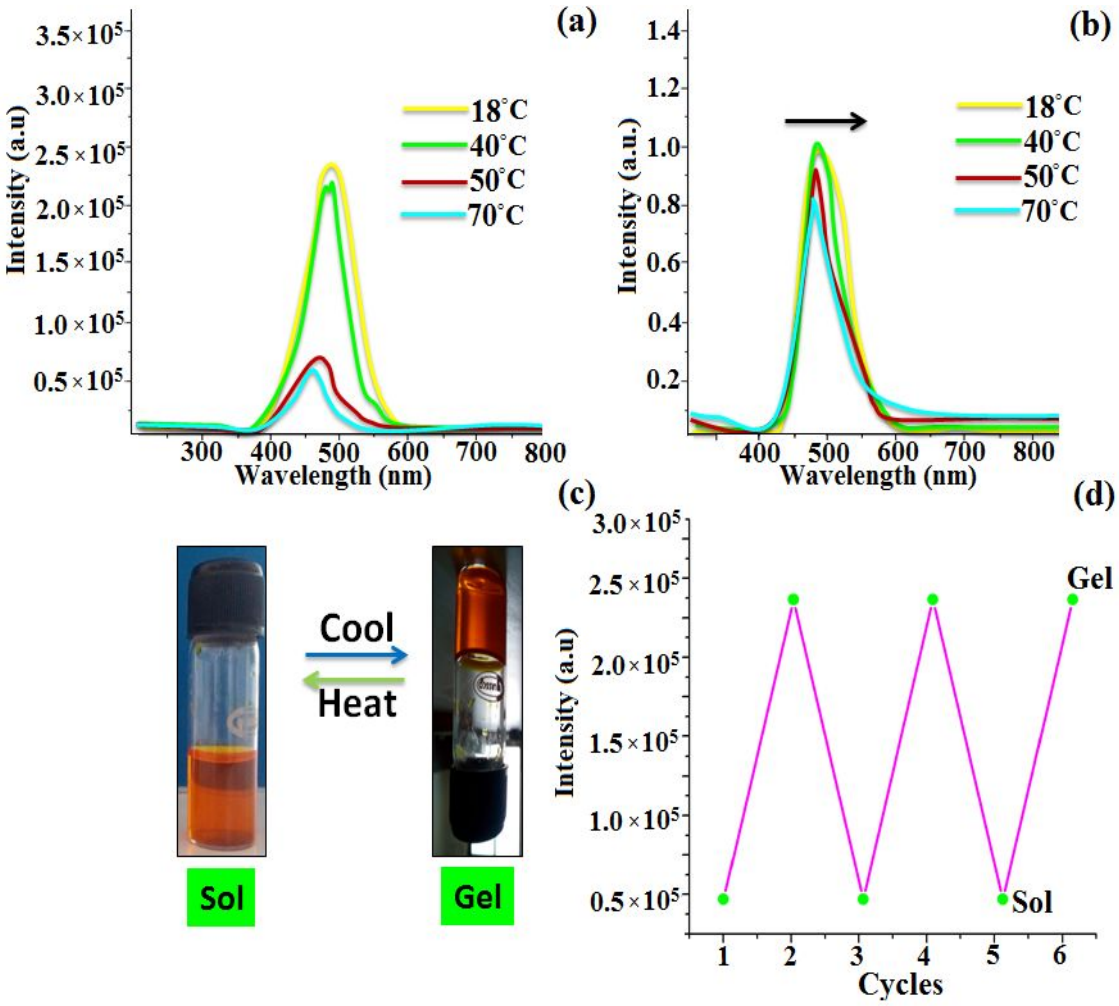

Figure S18. Emission spectra of compound **10c** showing an increase in the emission intensity on decreasing temperature due to gelation (a); normalized emission spectra showing a red shift on gelation (b); image of formation of gel from solution (c); reproducible reversibility of emission intensity in solution to gel interconversion (d).

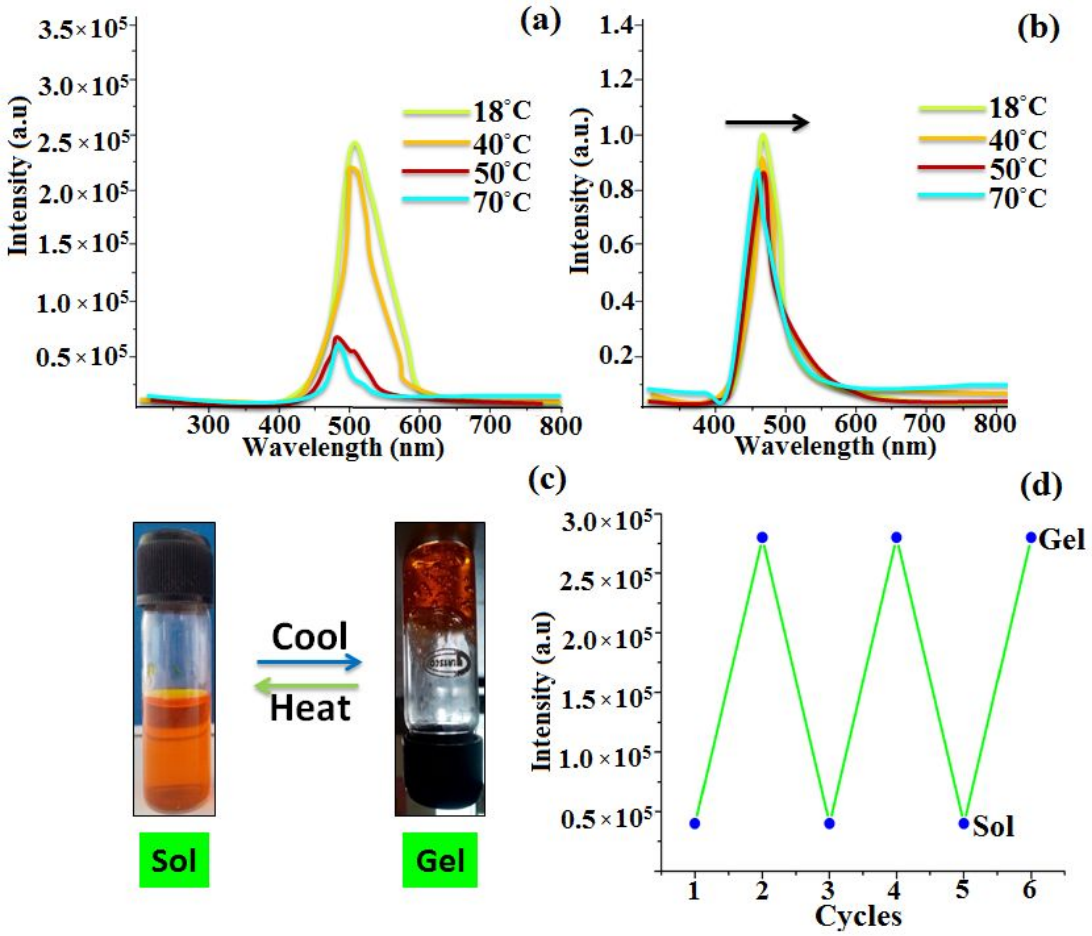

Figure S19. Emission spectra of compound **10d** showing an increase in the emission intensity on decreasing temperature due to gelation (a); normalized emission spectra showing a red shift on gelation (b); image of formation of gel from solution (c); reproducible reversibility of emission intensity in solution to gel interconversion (d).

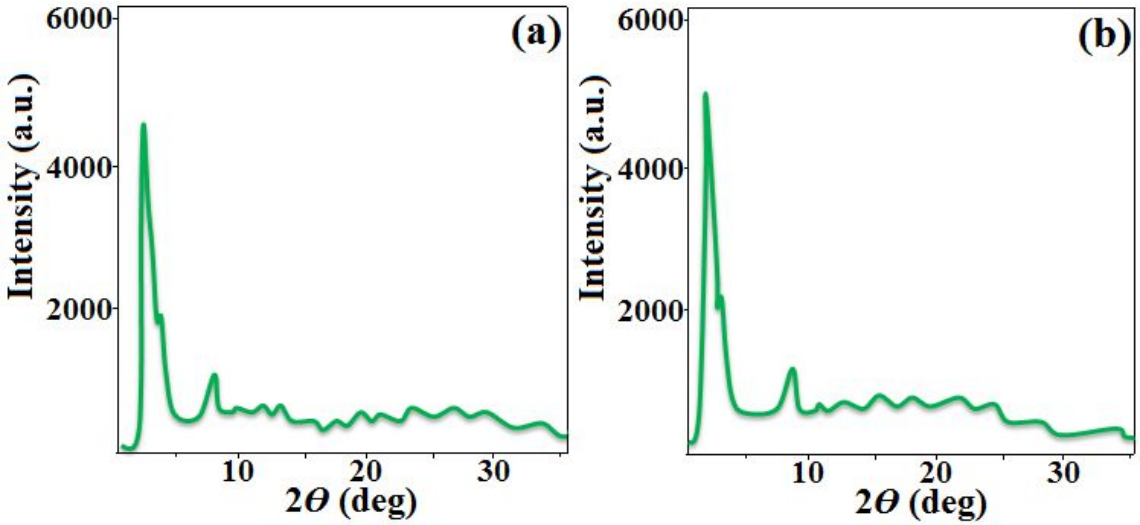

Figure S20. XRD profile depicting the intensity against the 2θ obtained for the Col_r phase of compounds **10c** (a); compound **10d** (b) in xerogels state.

Table S_3. Results of (hkl) indexation of XRD profiles of the compound **10c** in xerogel state at room temperature.

Compound (D/Å)	**Phase (T/°C)**	**dobs (Å)**	**Miller indices**	**Lattice Parameters (Å)**
10c	Colr (RT)	32.76	200	
		20.26	110	
		10.38	340	a = 65.22
		7.05	240	b = 28.97
		4.49	440	
		3.77	520	
		3.18	630	

Table S_4. Results of (hkl) indexation of XRD profiles of the compound **10d** in xerogel state at room temperature.

Compound (D/Å)	**Phase (T/°C)**	**dobs (Å)**	**Miller indices**	**Lattice Parameters (Å)**
		34.06	200	
		20.18	110	
		10.38	320	a = 63.72

10d	Colr (RT)	7.05	240	b = 28.85
		4.69	430	
		3.77	540	
		3.18	640	

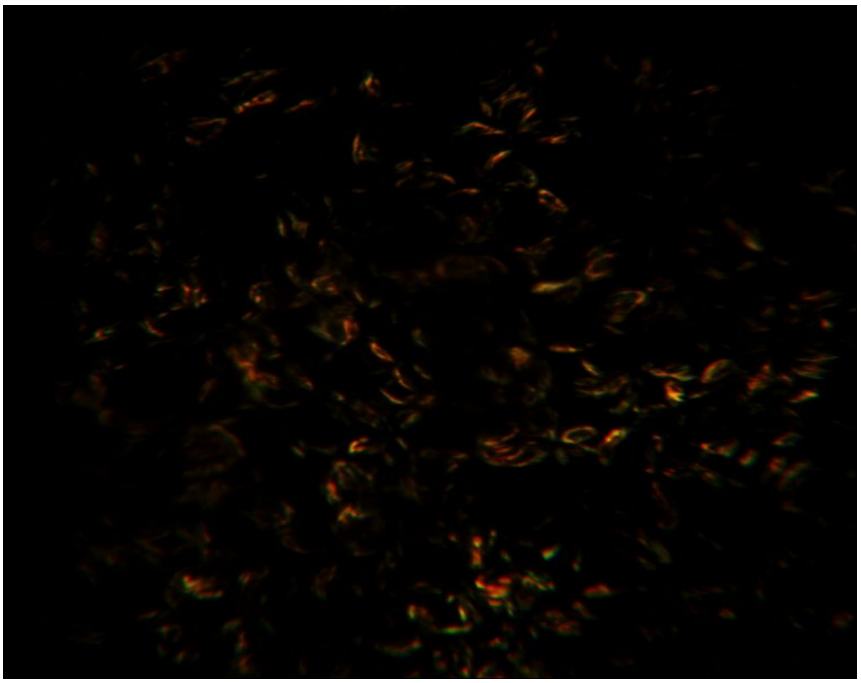

Figure S21. POM image of the xerogel showing a birefringent texture of comp.**10C**.

Table S_5. Electroluminescent performance data of OLEDs[a]

Doping concentration (wt.%)	Vonse[b] (V)	η_p[c] (lmW^{-1})	η_c[d] (cdA^{-1})	EQE[e] (%)	CIE (x,y)[f]	Lmax[g] (cd/m^2)	λem[h] (nm)
1	6.2	0.2	0.6	0.8	(0.24, 0.33)	438	496
2	6.7	0.1	0.6	0.6	(0.24, 0.33)	407	494
5	7.2	0.2	0.3	0.6	(0.24, 0.33)	353	496
6	6.9	0.2	0.5	0.3	(0.24, 0.32)	314	482
Neat	7.4	0.2	0.6	0.4	(0.24, 0.31)	286	484

[a]:Device configuration ITO/PEDOT/emissive layer or doped with CBP/TPBi/LIF/Al, bVonset: turn-on voltage at luminance of 100 cd/m^2. Power efficiency (η_p), current efficiency (η_c). EQE[e]: external quantum efficiency, CIE (x,y)[f]: Colour coordinates, Lmax[g]: maximum luminance of the device, λem[h]: emission maximum wavelength.

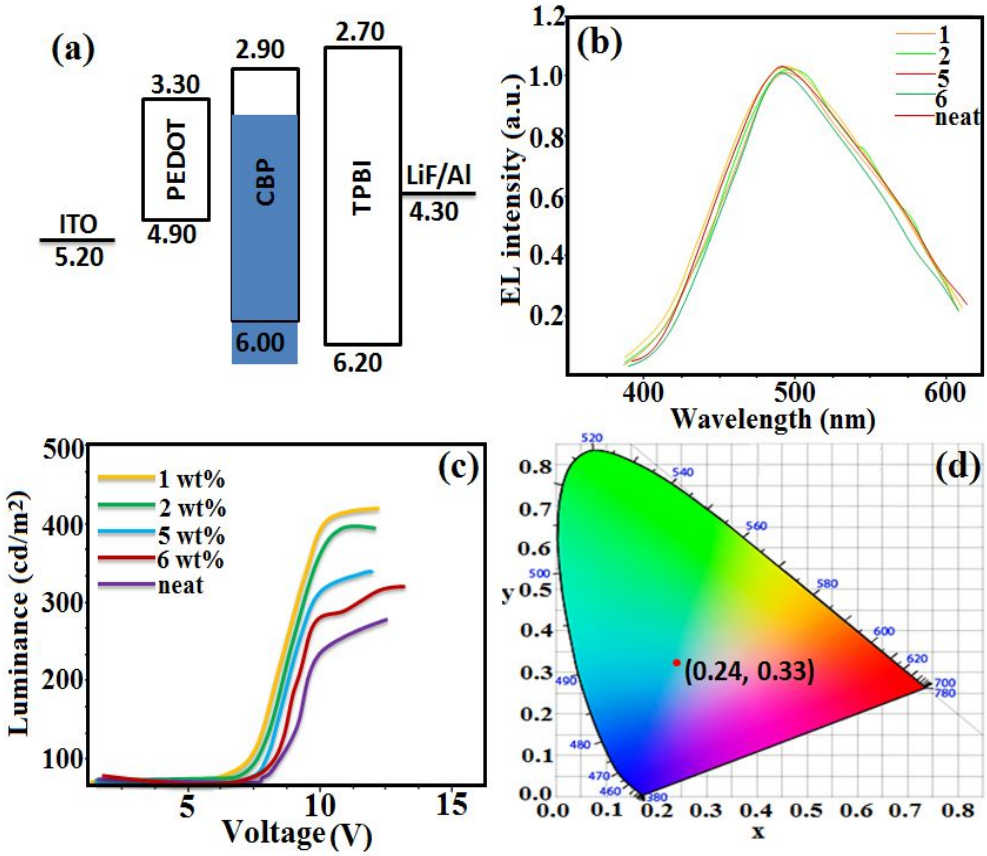

Figure S22. (a) Energy-level diagram of the compound **10c** used for the fabrication of (CBP) host OLED device configuration as ITO/PEDOT/emissive layer/TPBi/LiF/Al, (b) EL spectra of OLED devices with various doping concentrations and neat film of compound **10c**, (c) luminance vs voltage plots of the solution proceed OLED device at different doping concentrations and (d) CIE chromatogram of dye doped compound **10c** (1 wt.%) of the device.

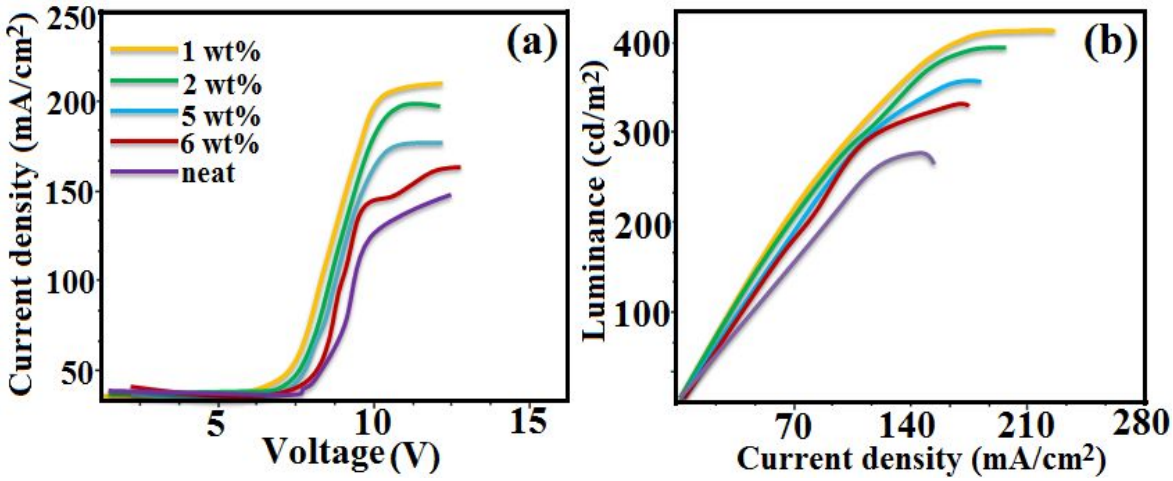

Figure S23. (a) Current density vs voltage, (b) luminance vs current density of OLED devices at different doping concentrations of compound **10c**.

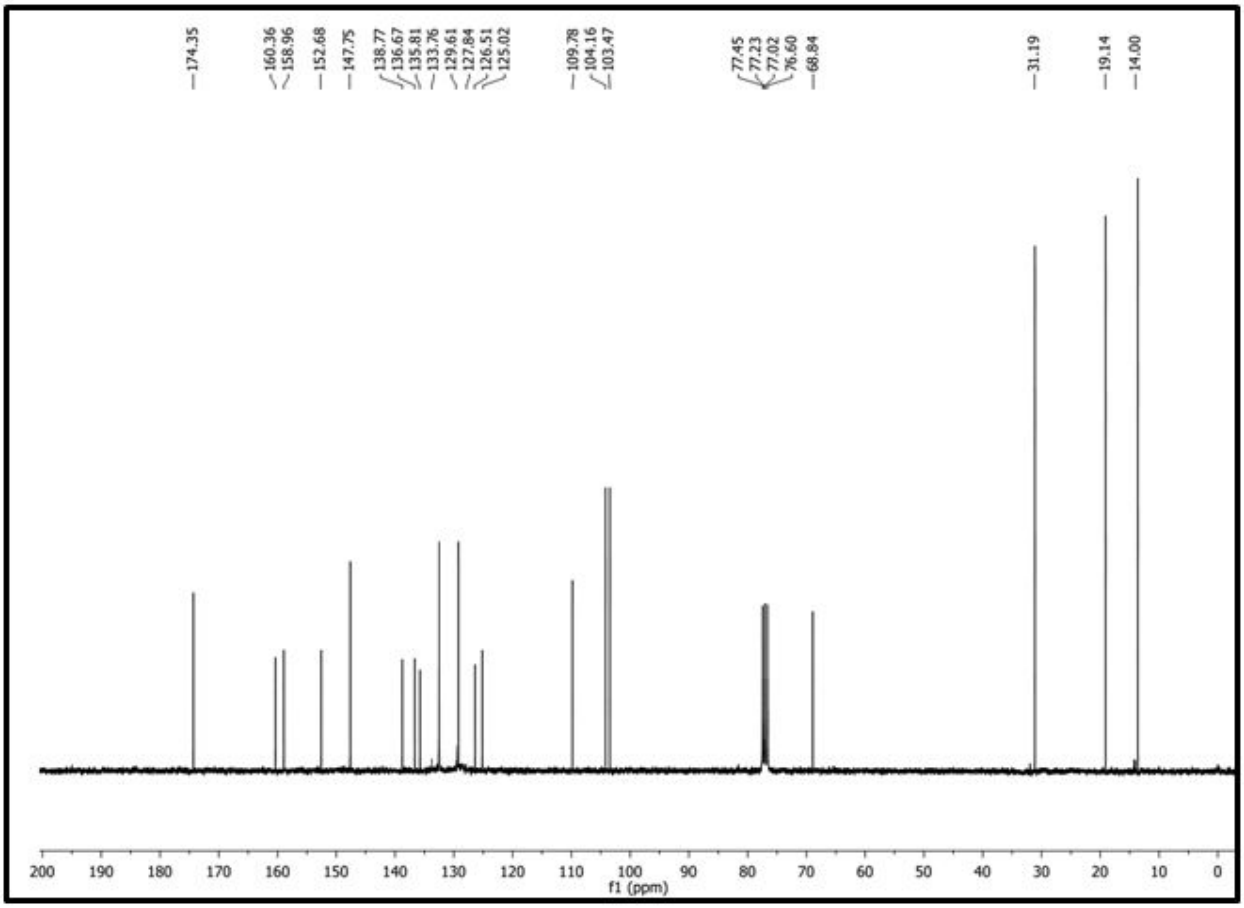

Figure S24. ^{13}C NMR of compound **8a**

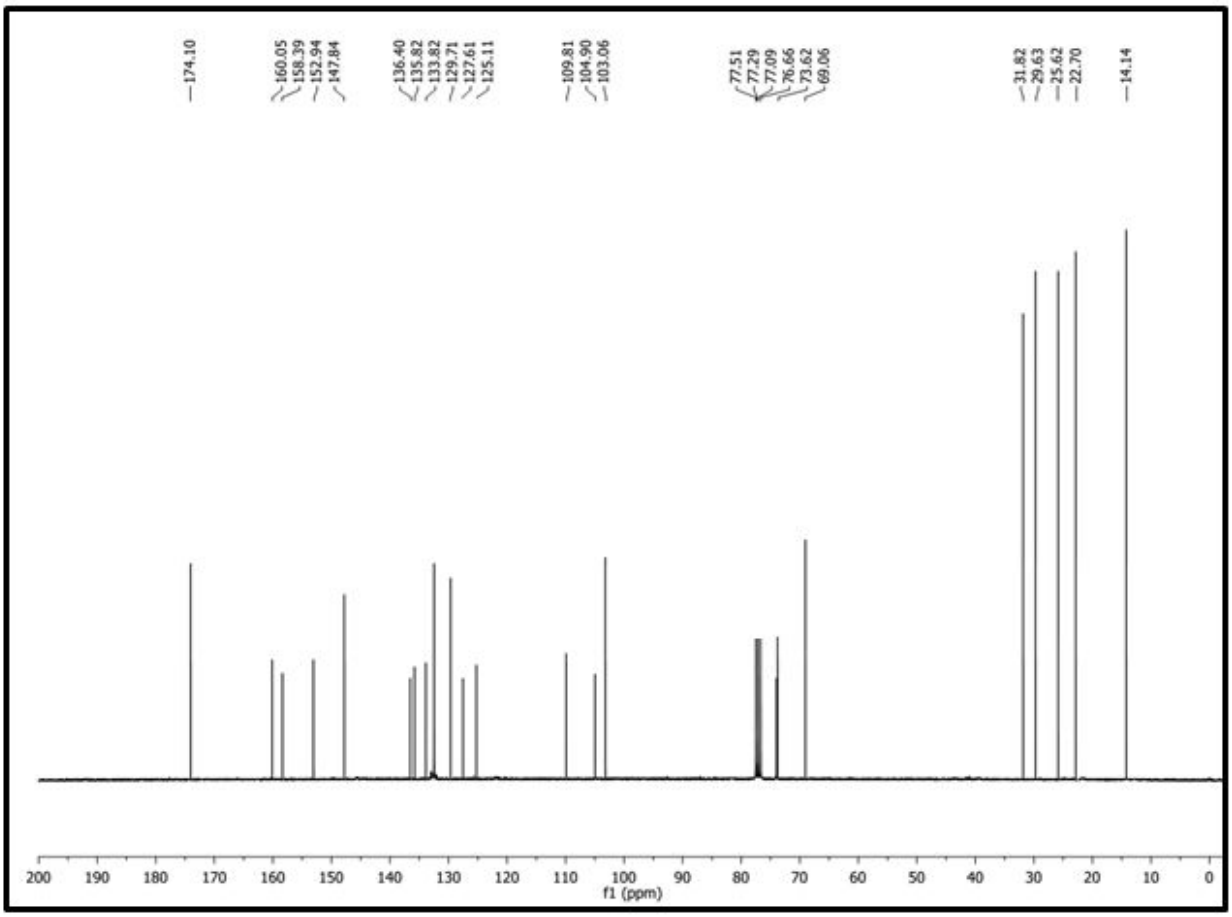

Figure S25. ^{13}C NMR of compound **8b**

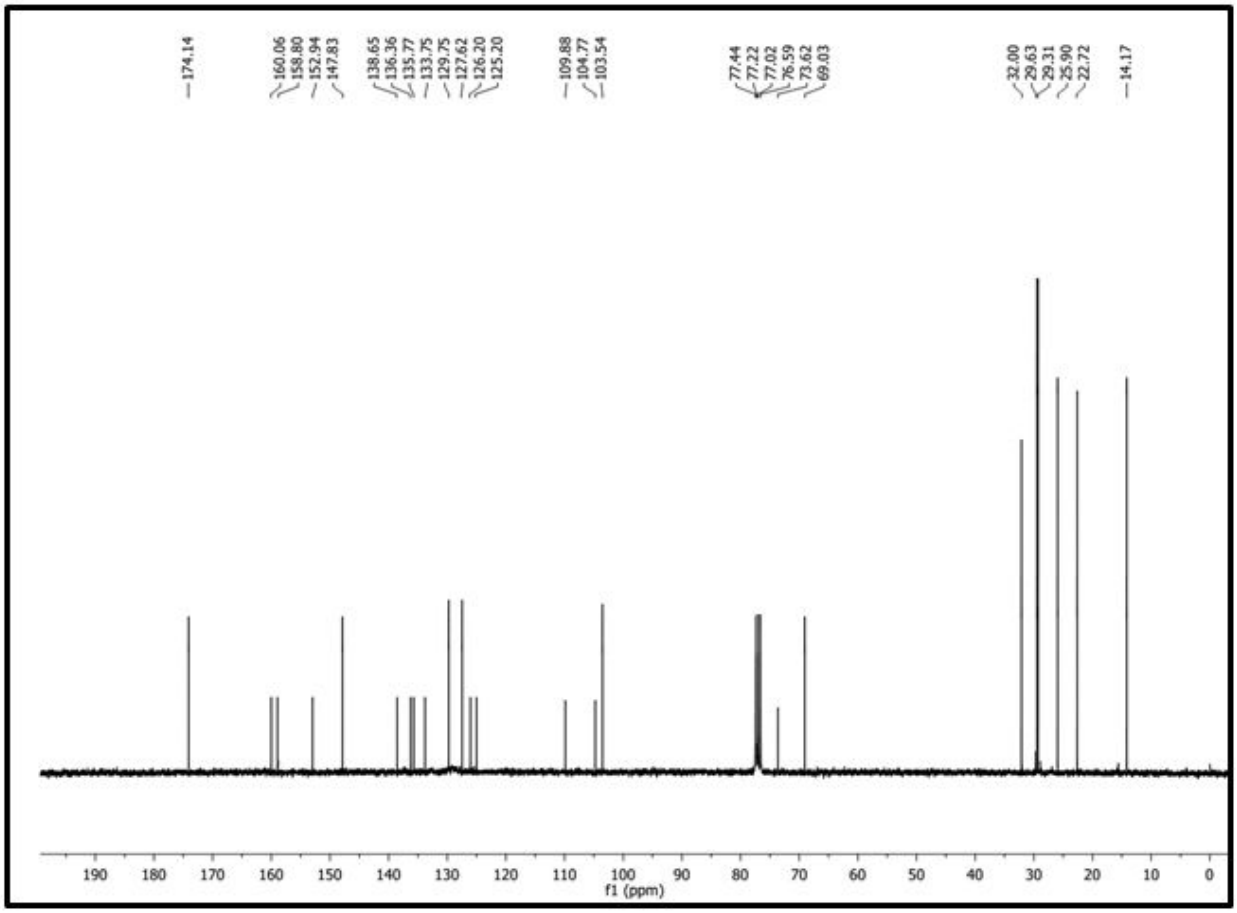

Figure S26. ^{13}C NMR of compound **8c**

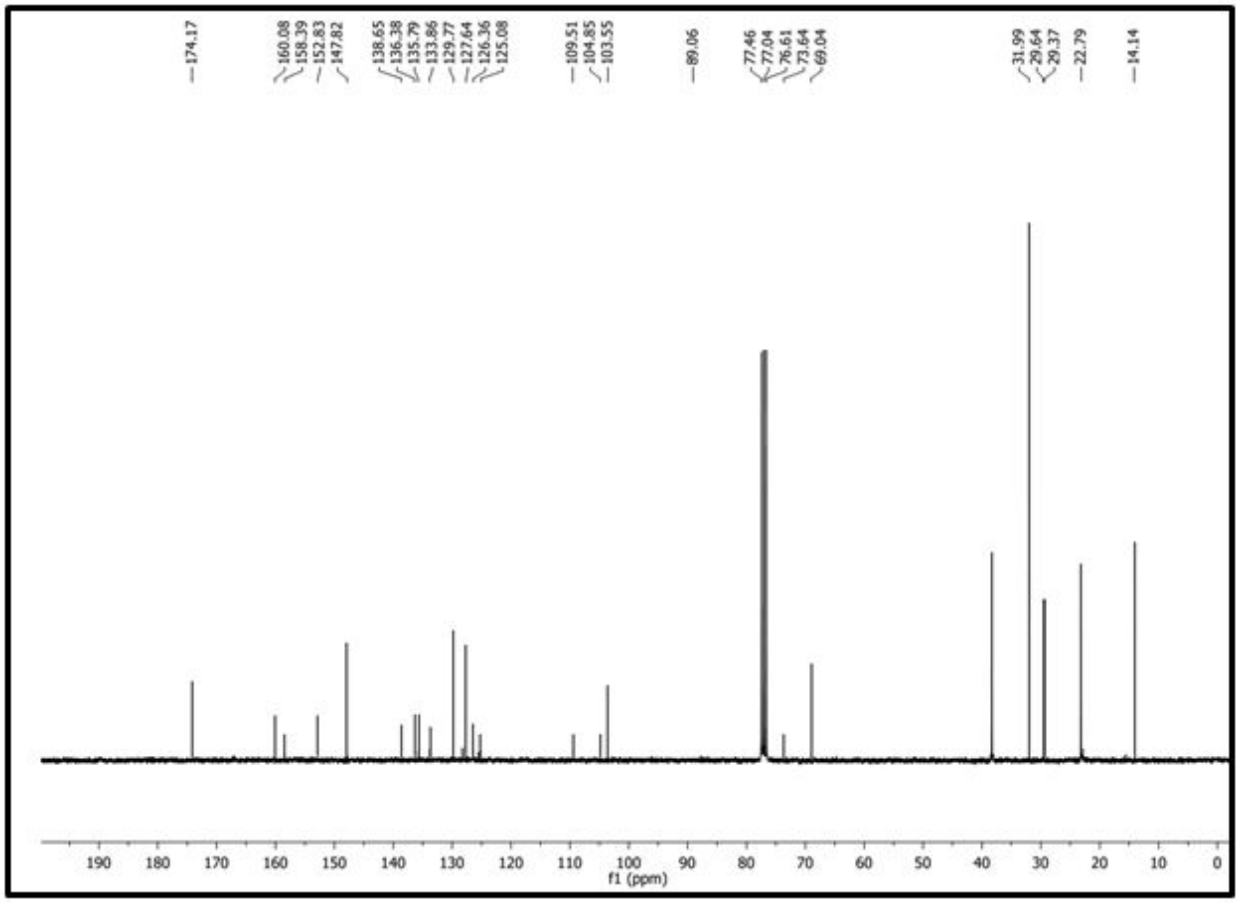

Figure S27. ^{13}C NMR of compound **8d**

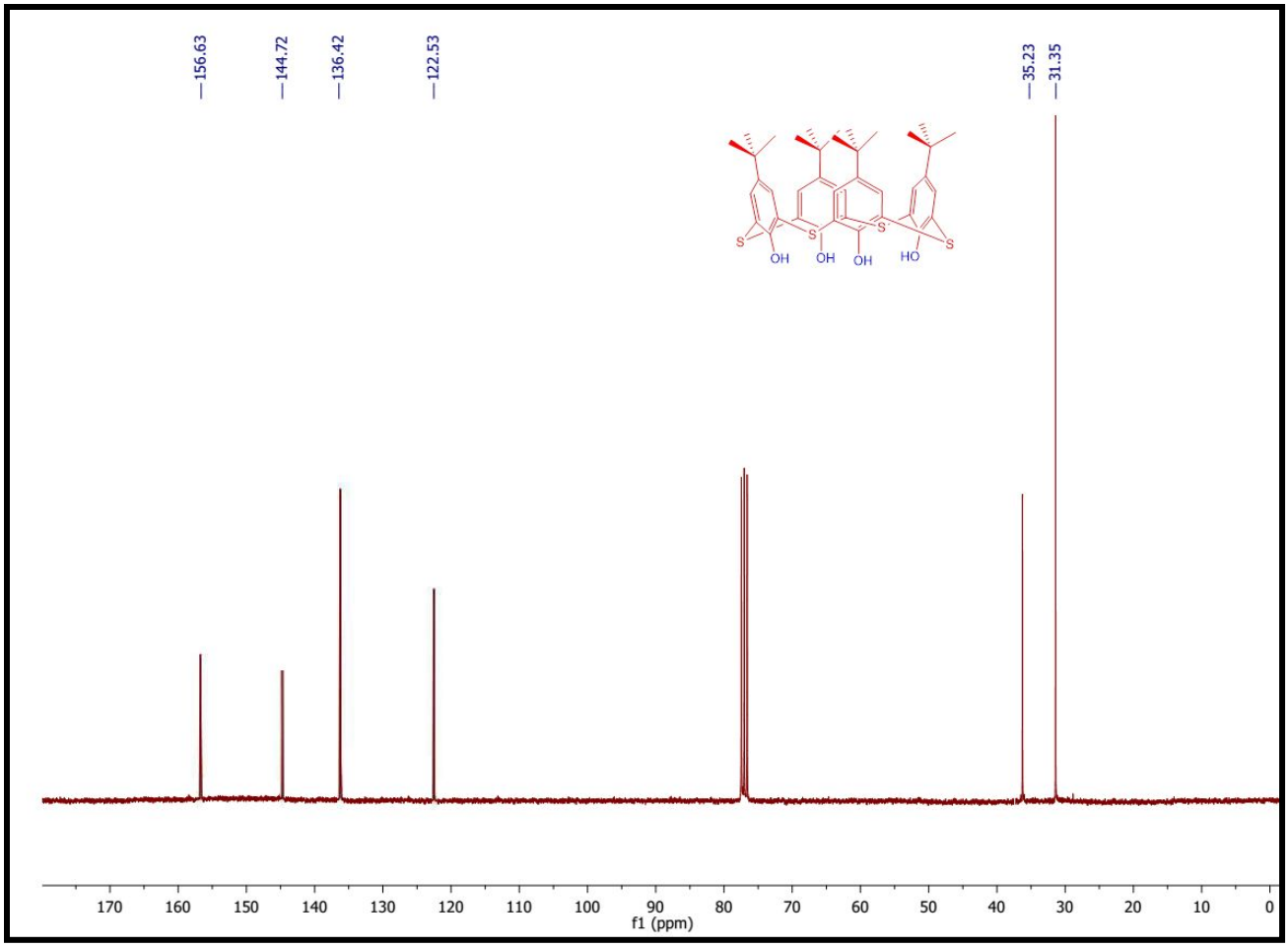

Figure S28. ^{13}C NMR of compound **9**

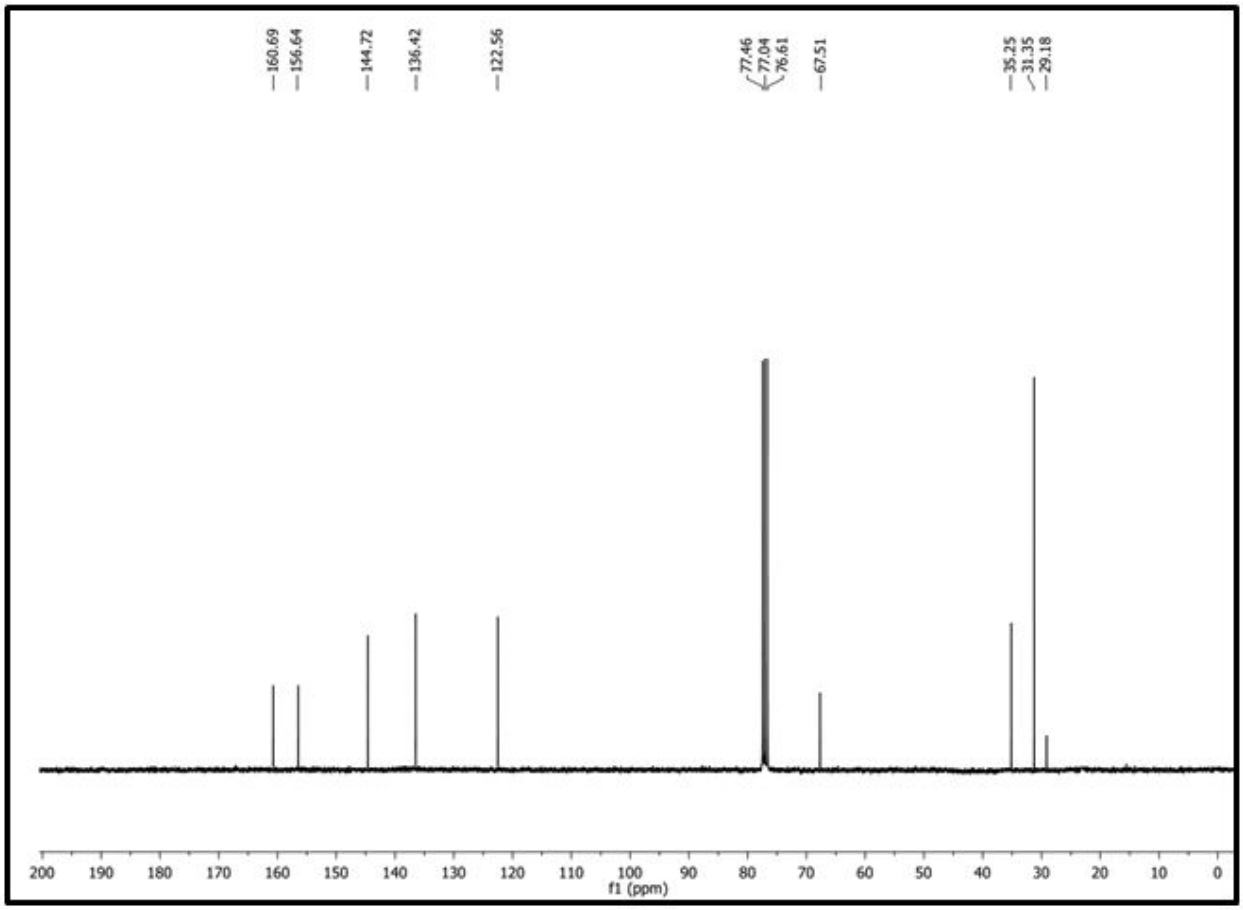

Figure S29. ^{13}C NMR of compound **9a**

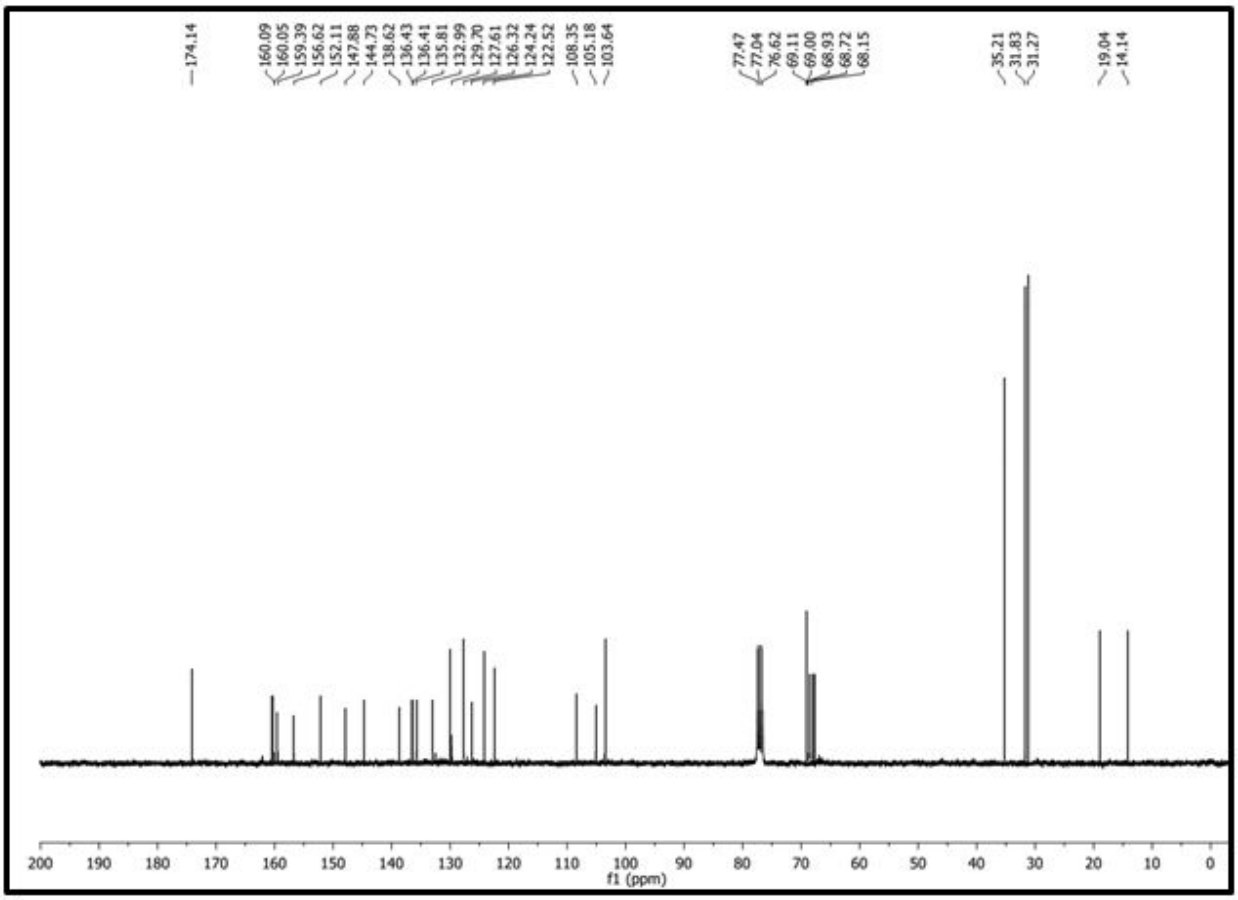

Figure S30. ^{13}C NMR of compound **10a**

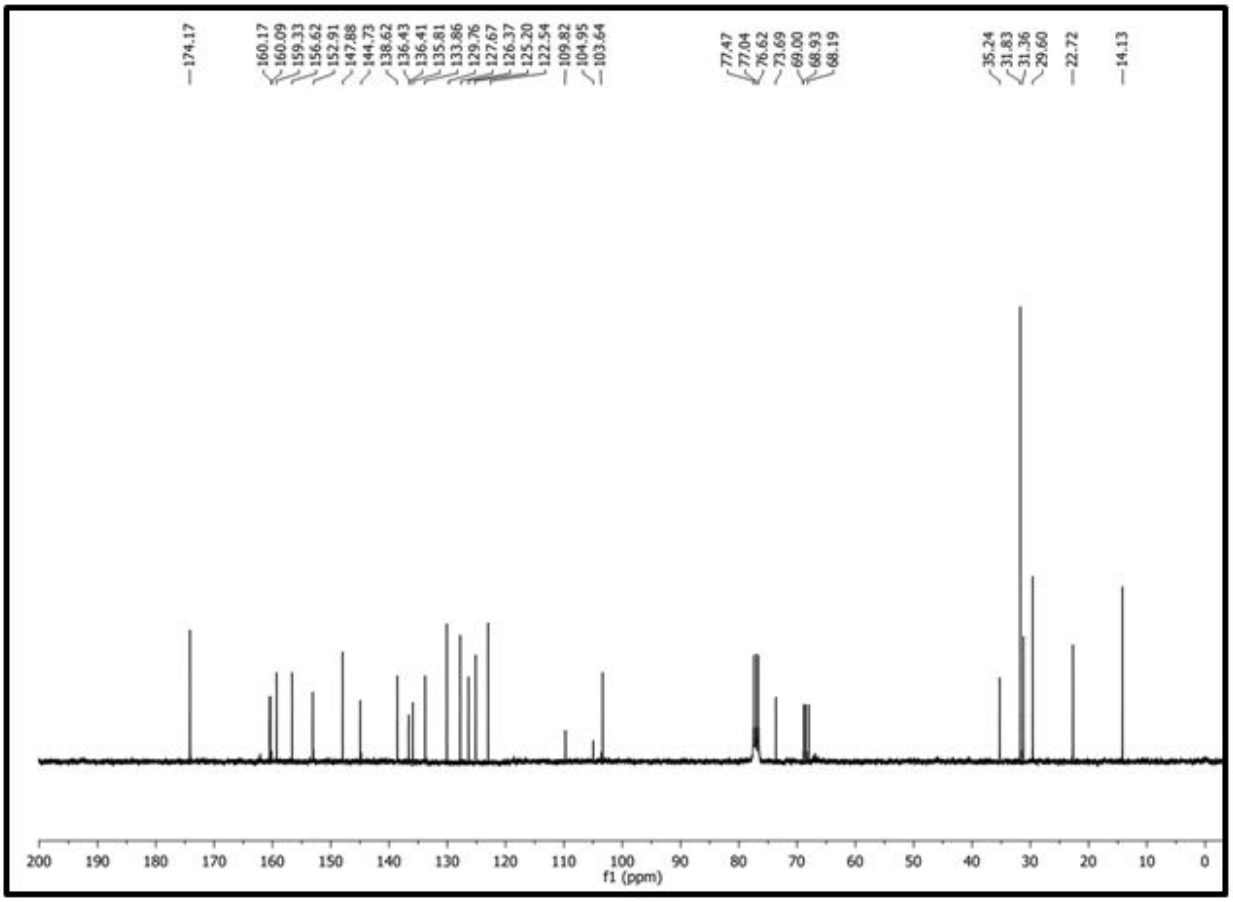

Figure S31. ^{13}C NMR of compound **10b**

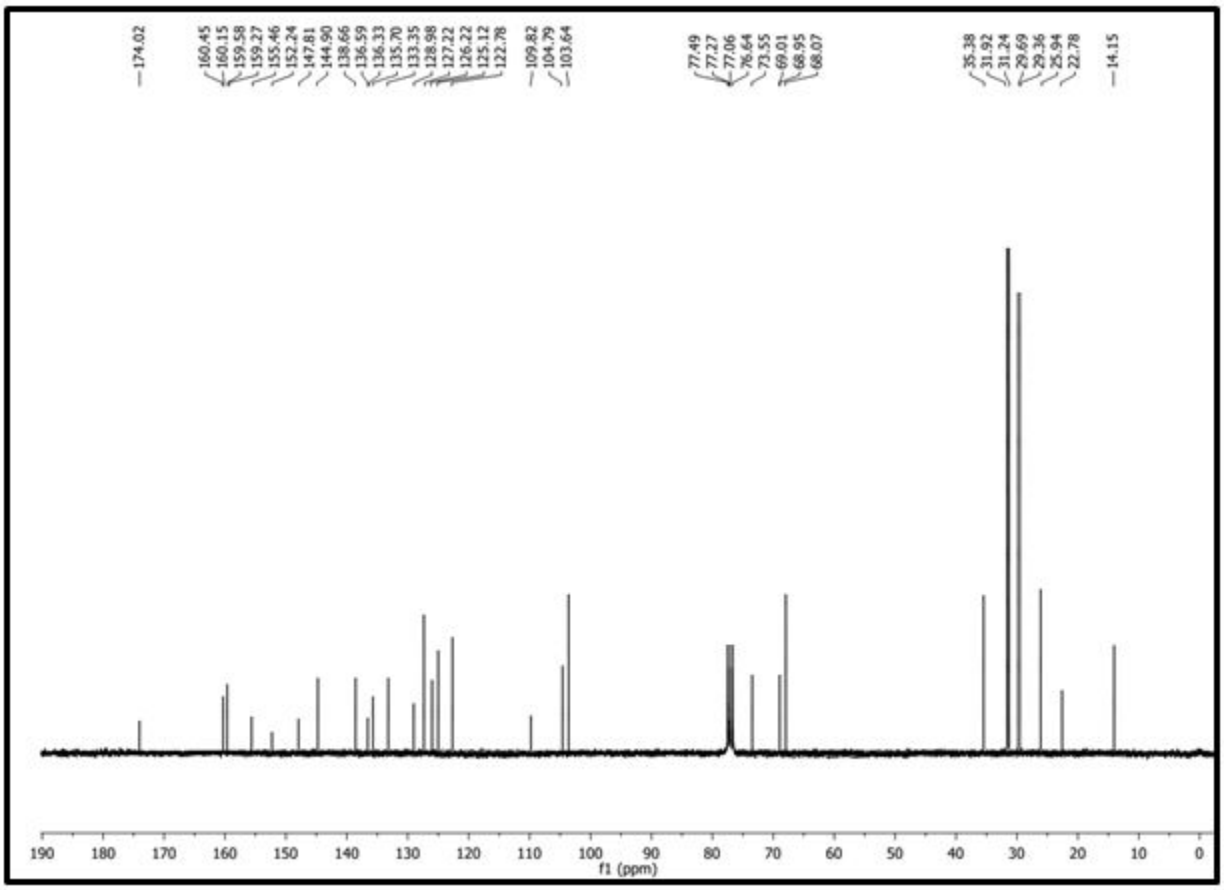

Figure S32. ^{13}C NMR of compound **10c**

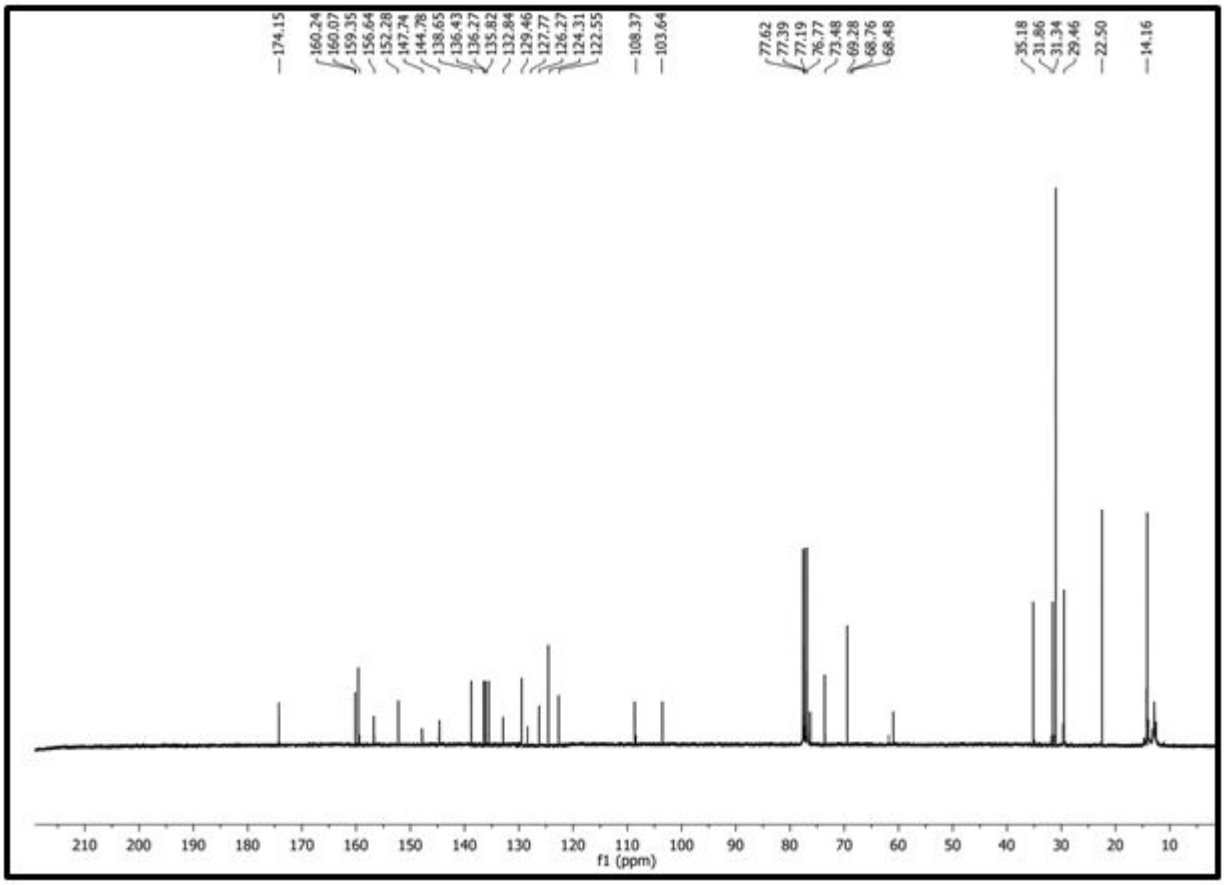

Figure S33. ^{13}C NMR of compound **10d**

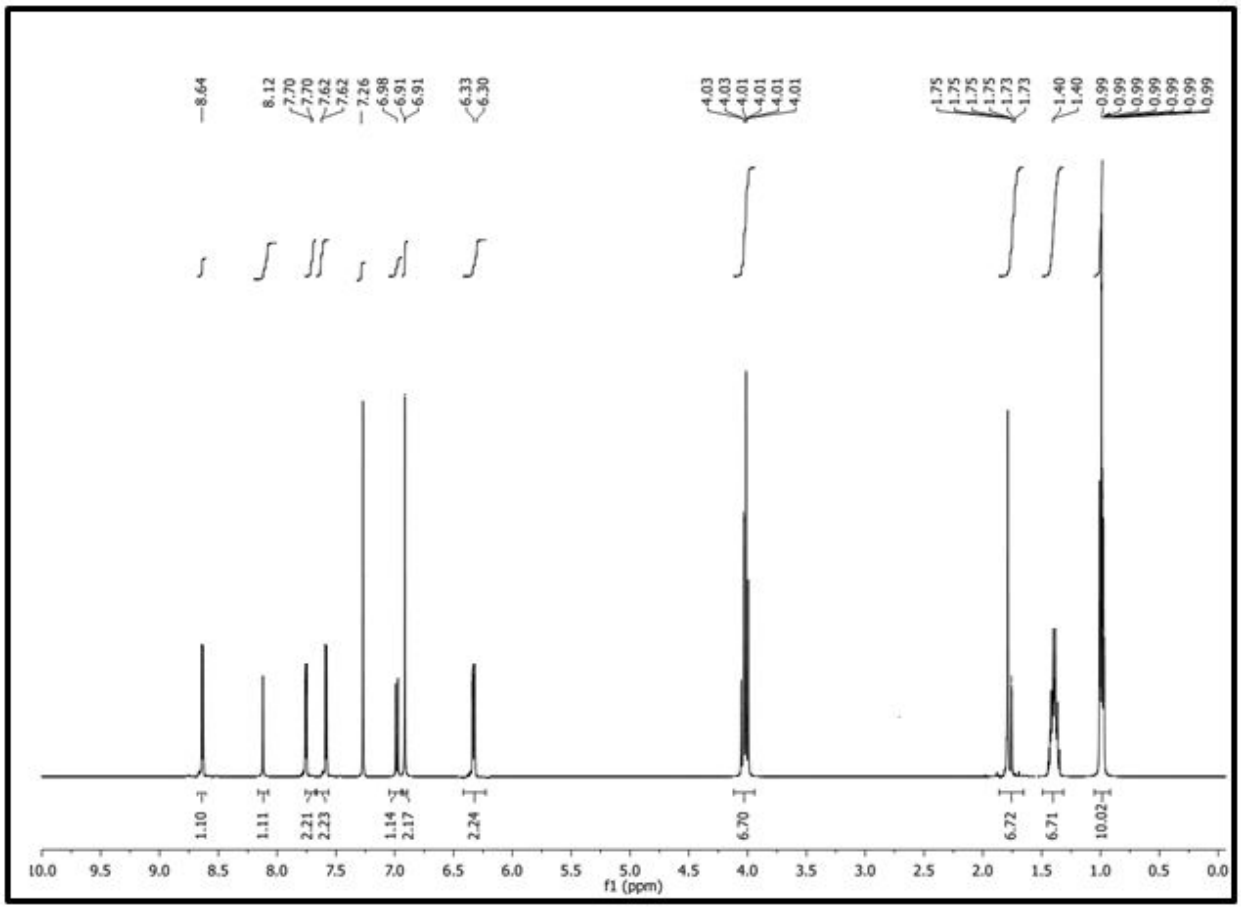

Figure S34. ^{1}H NMR of compound **8a**

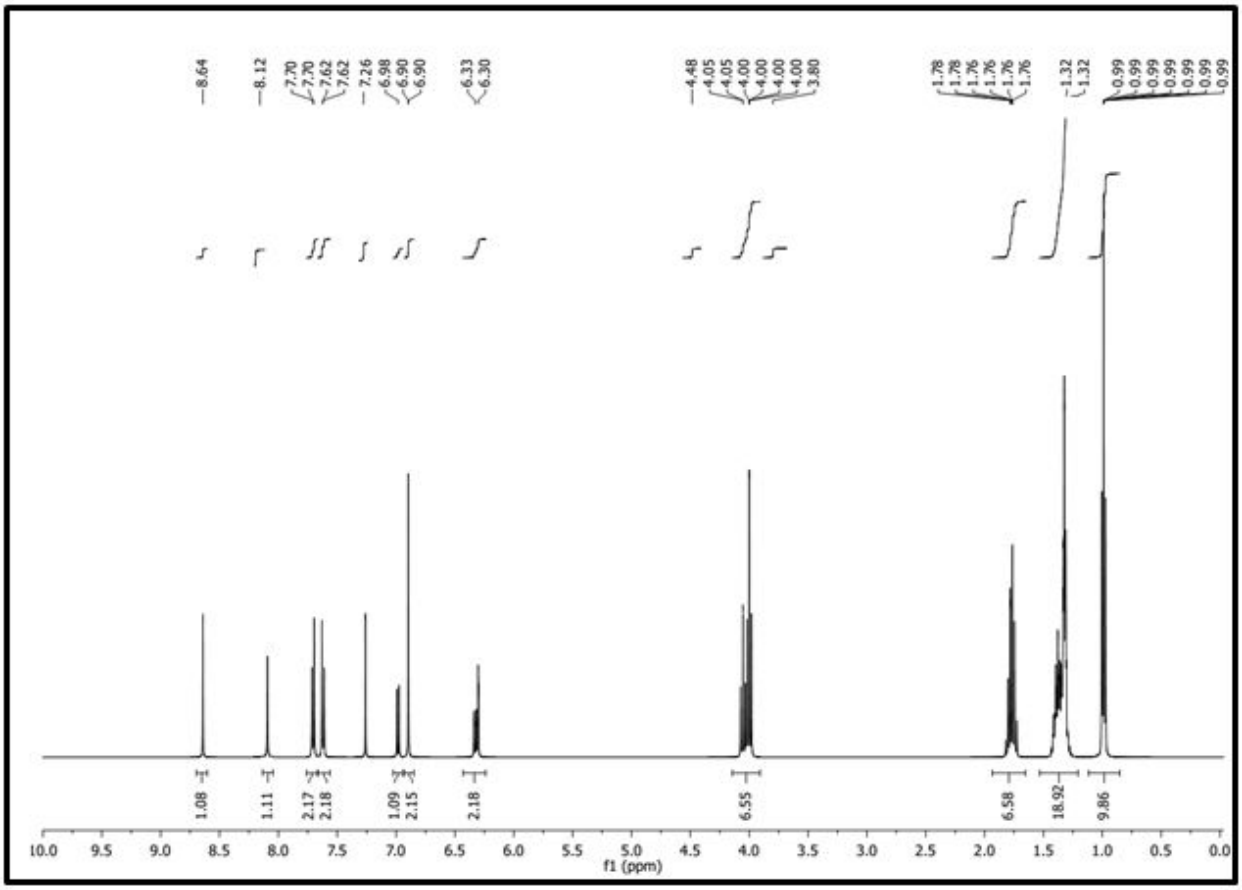

Figure S35. ^{1}H NMR of compound **8b**

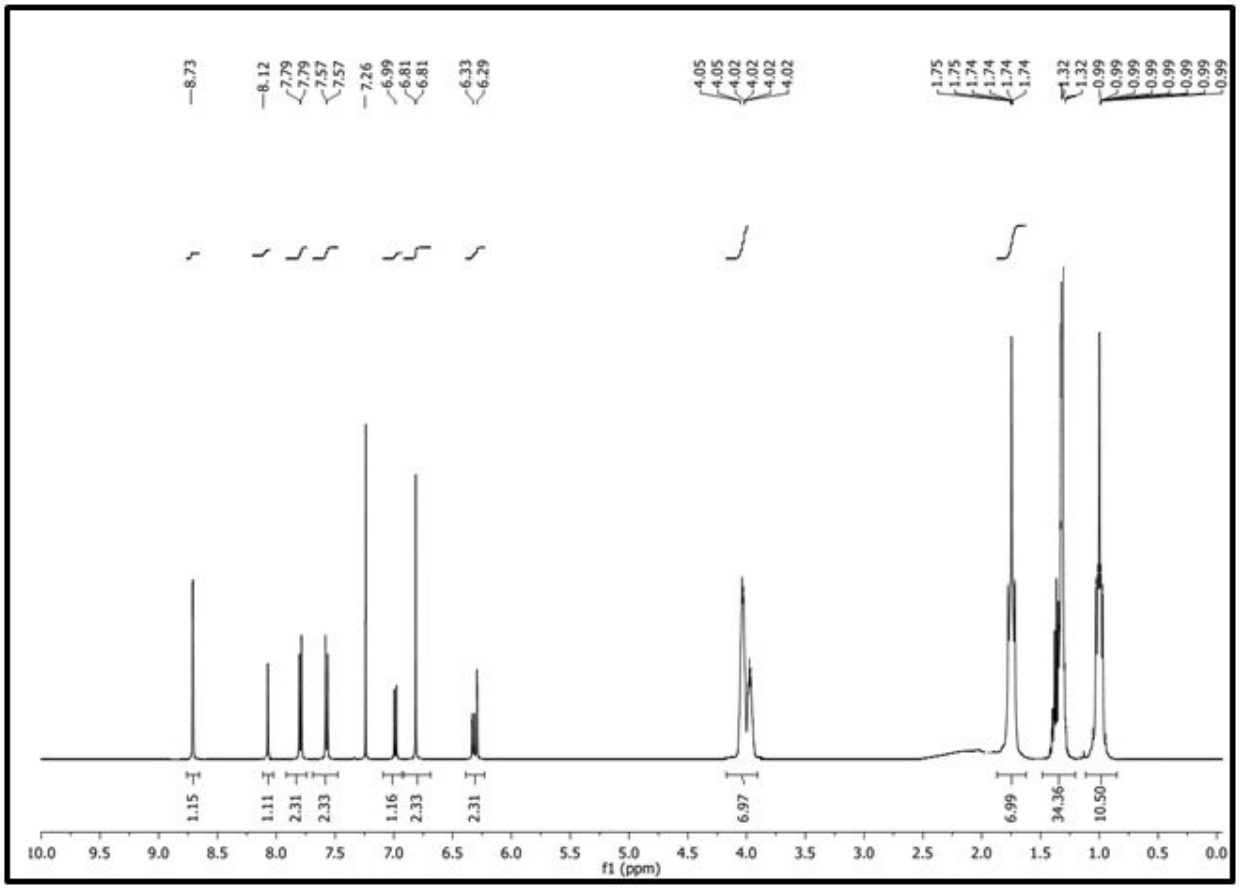

Figure S36. ^{1}H NMR of compound **8c**

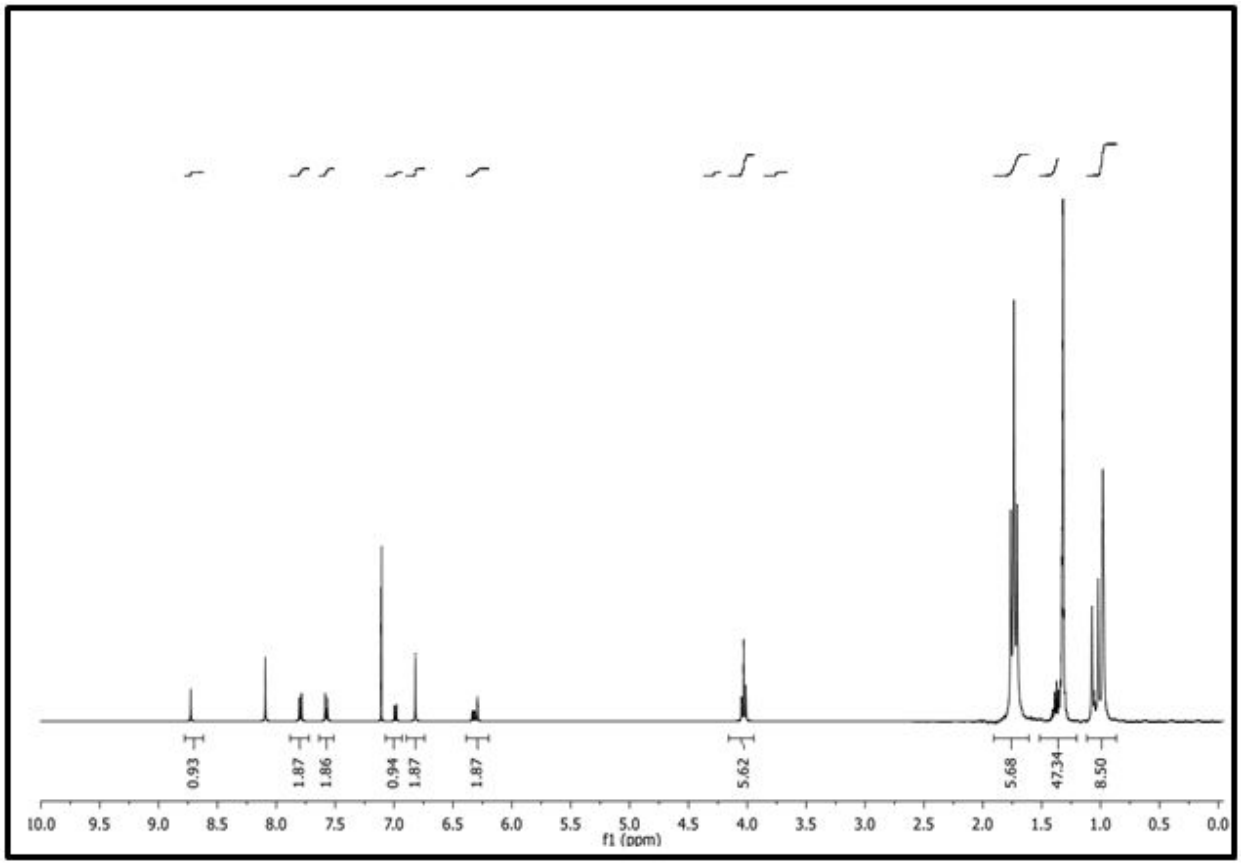

Figure S37. ^{1}H NMR of compound **8d**

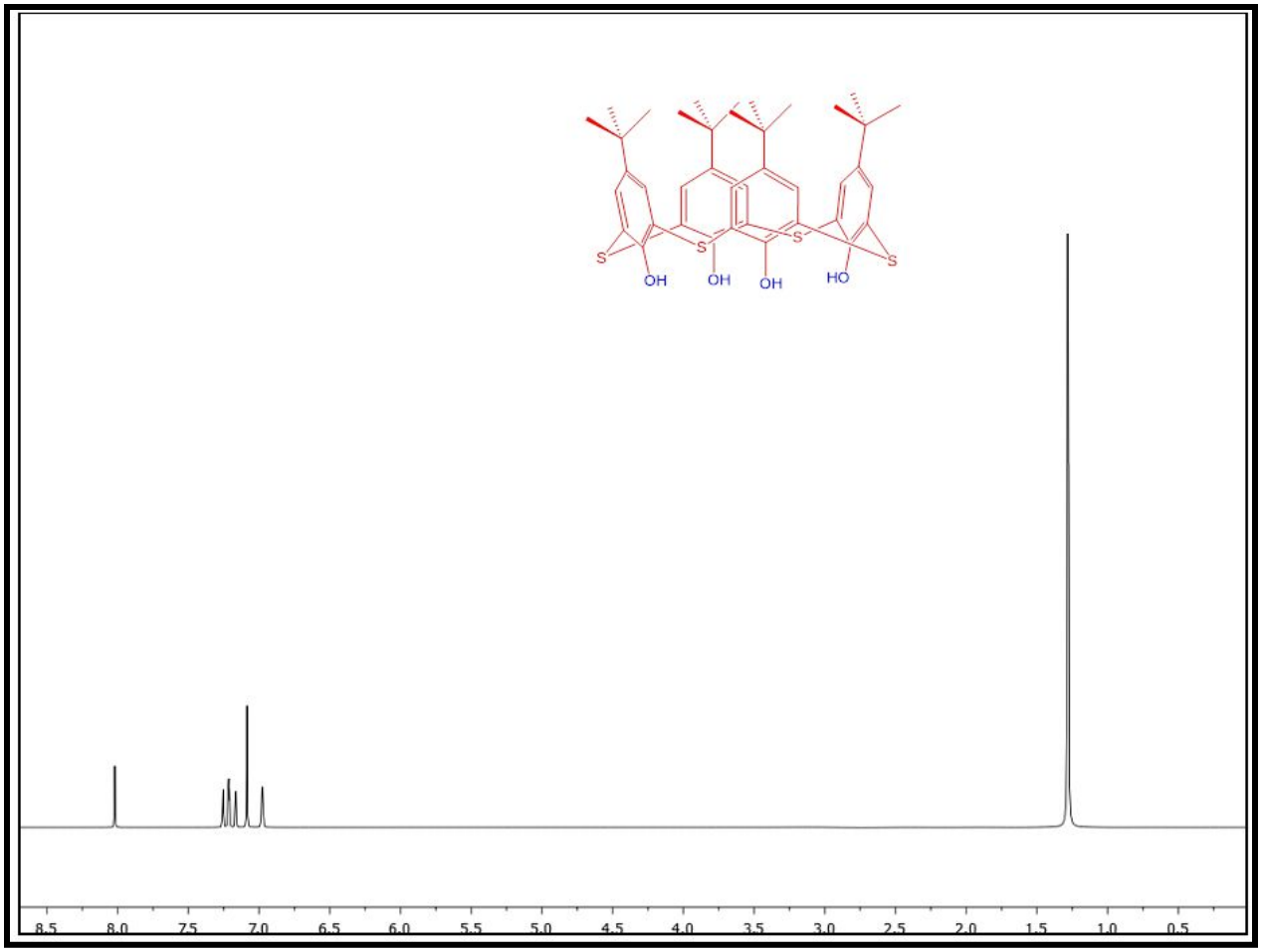

Figure S38. ^{1}H NMR of compound **9**

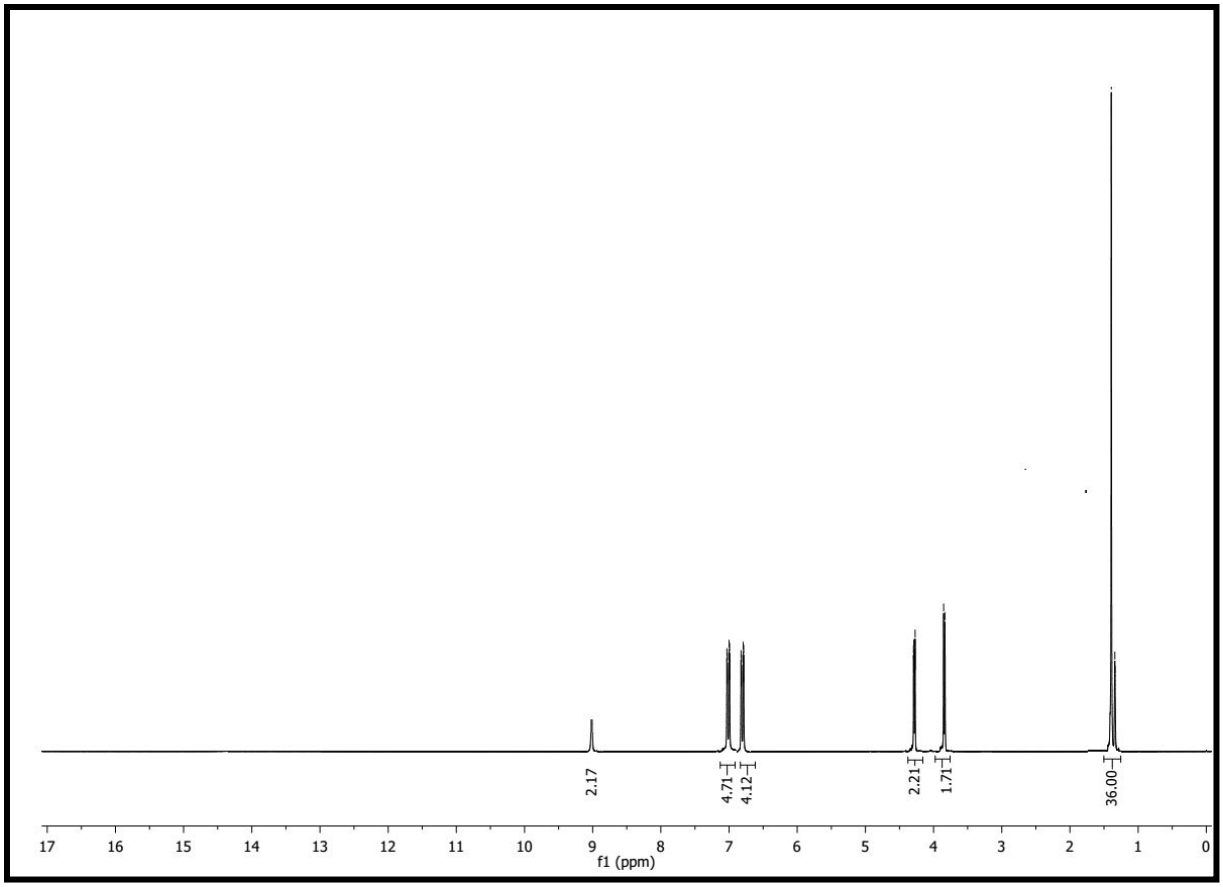

Figure S39. ^{1}H NMR of compound **9a**

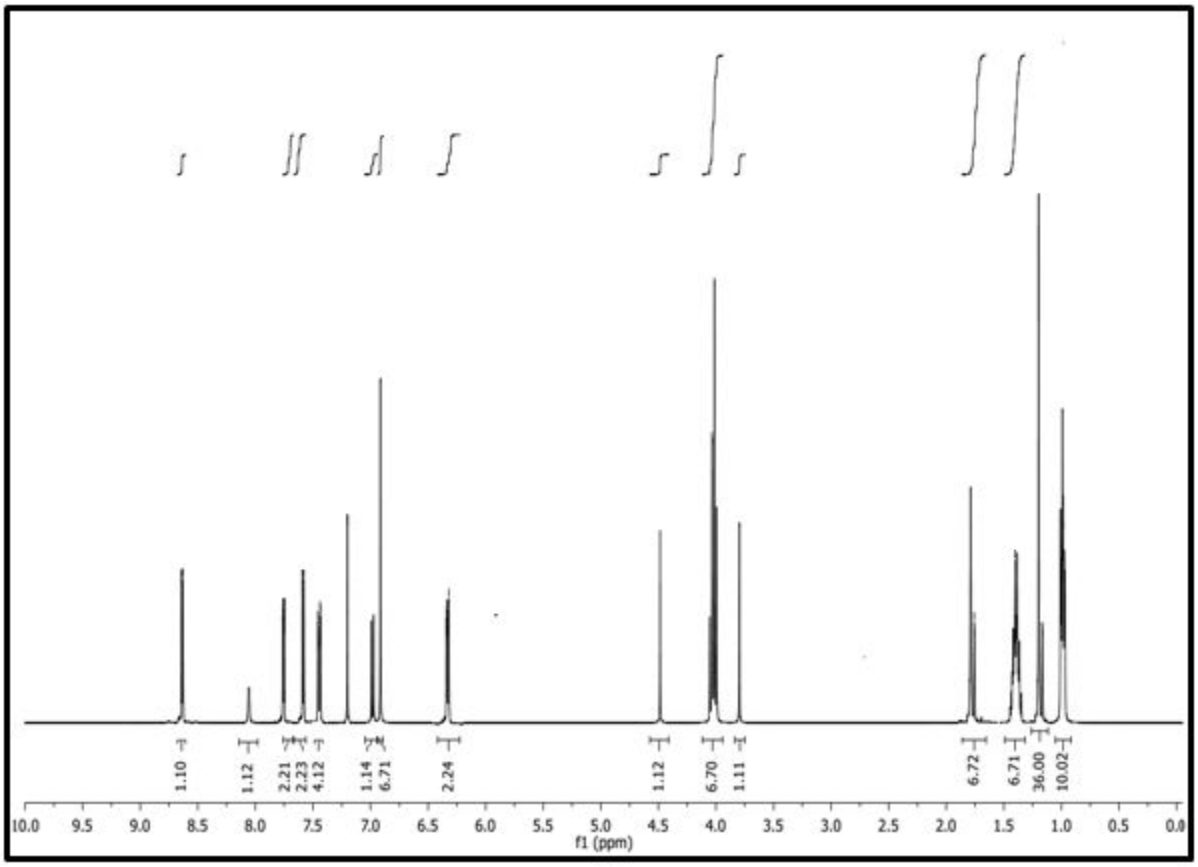

Figure S40. ^{1}H NMR of compound **10a**

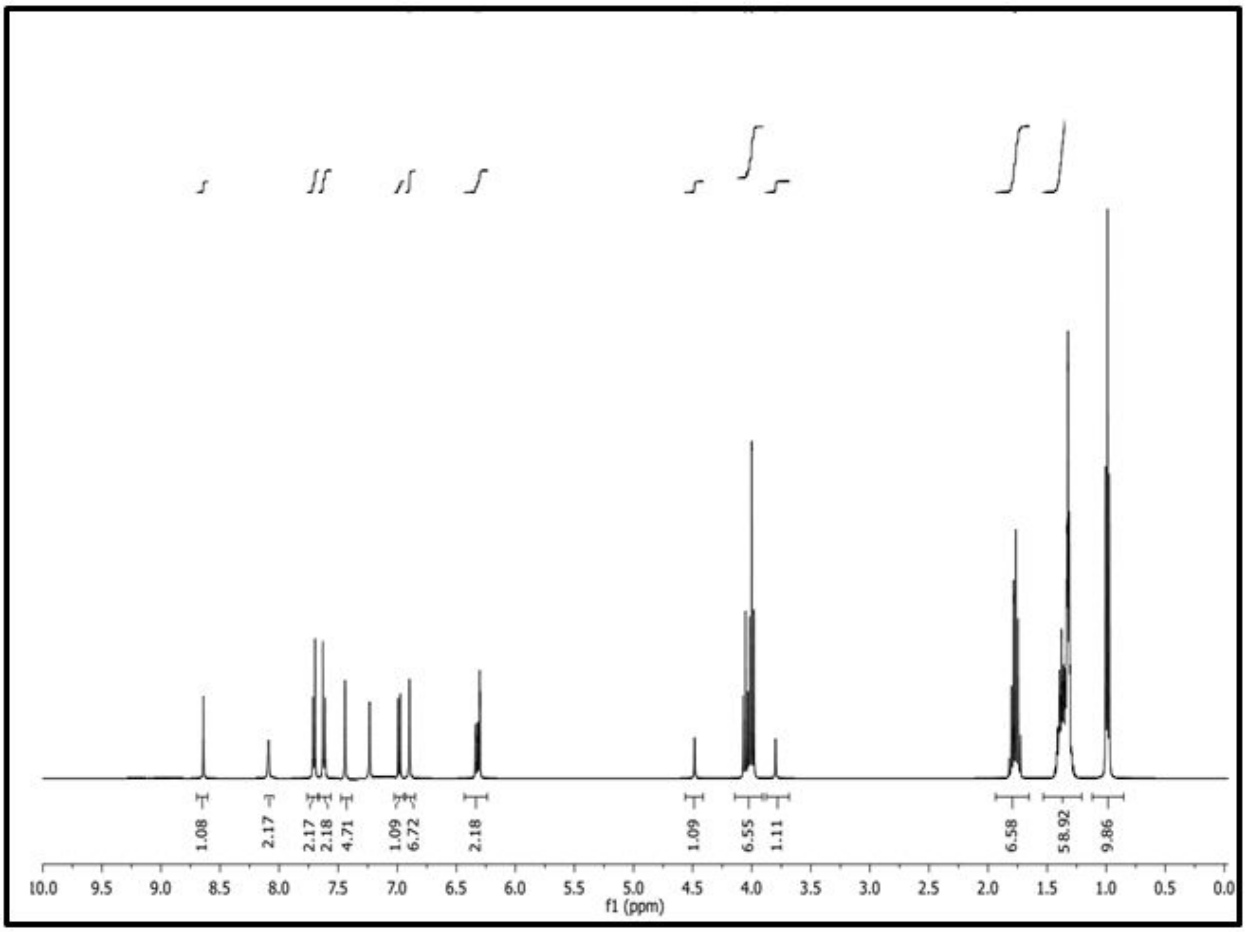

Figure S41. ^{1}H NMR of compound **10b**

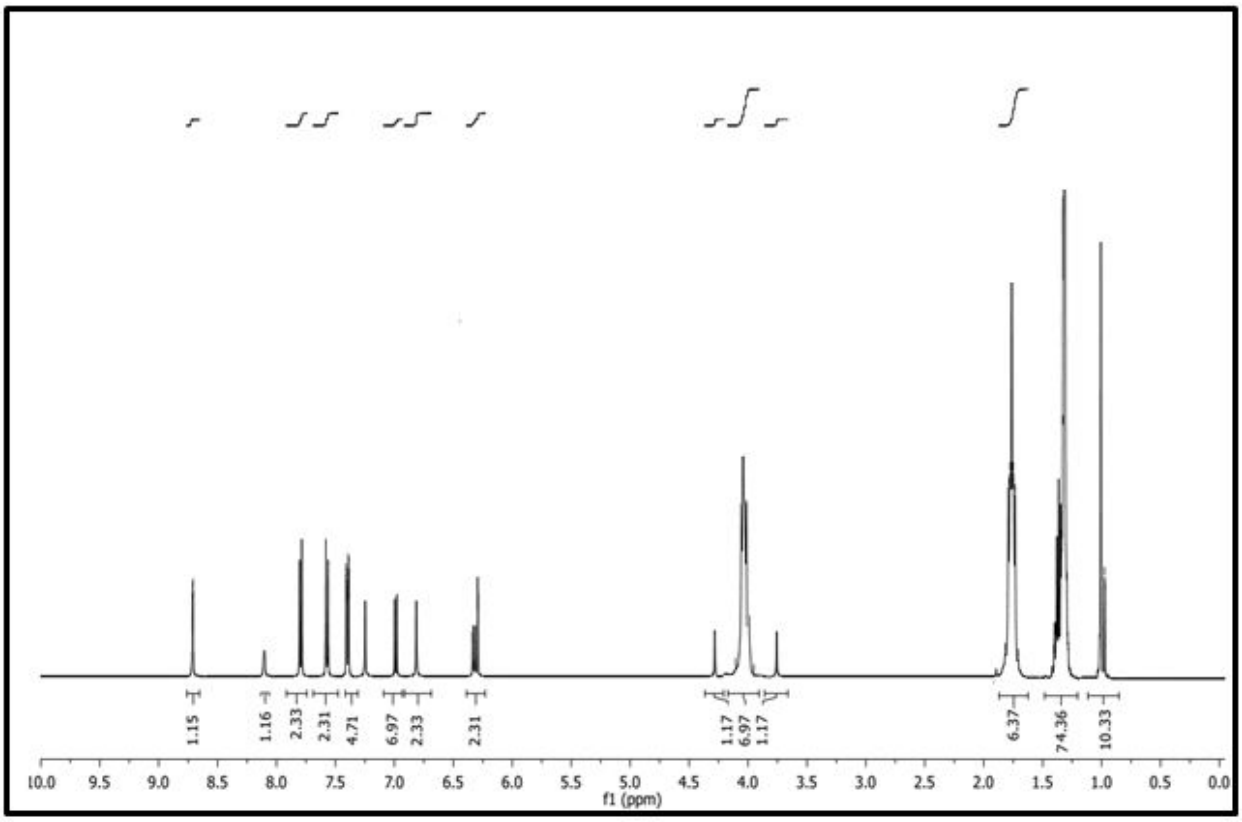

Figure S42. ^{1}H NMR of compound **10c**

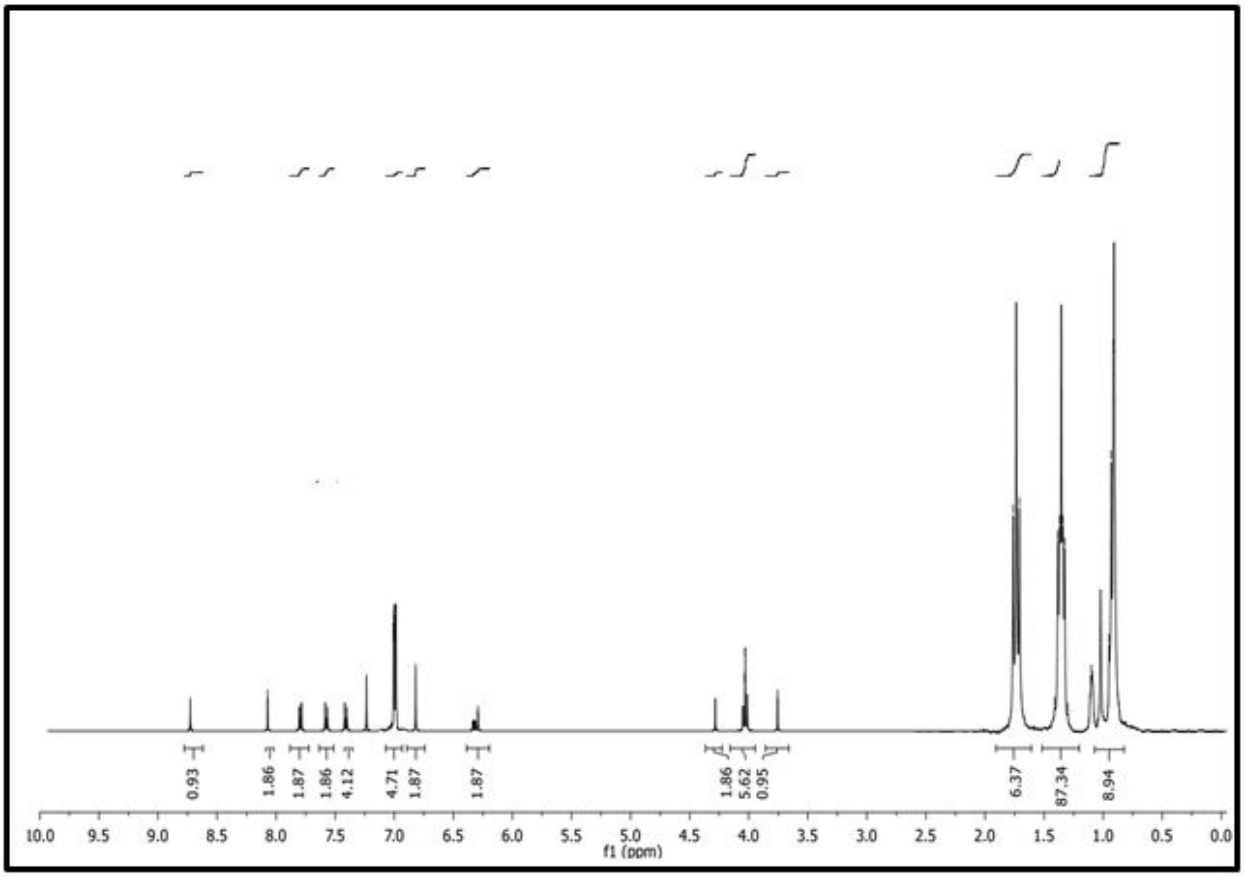

Figure S43. ^{1}H NMR of compound **10d**

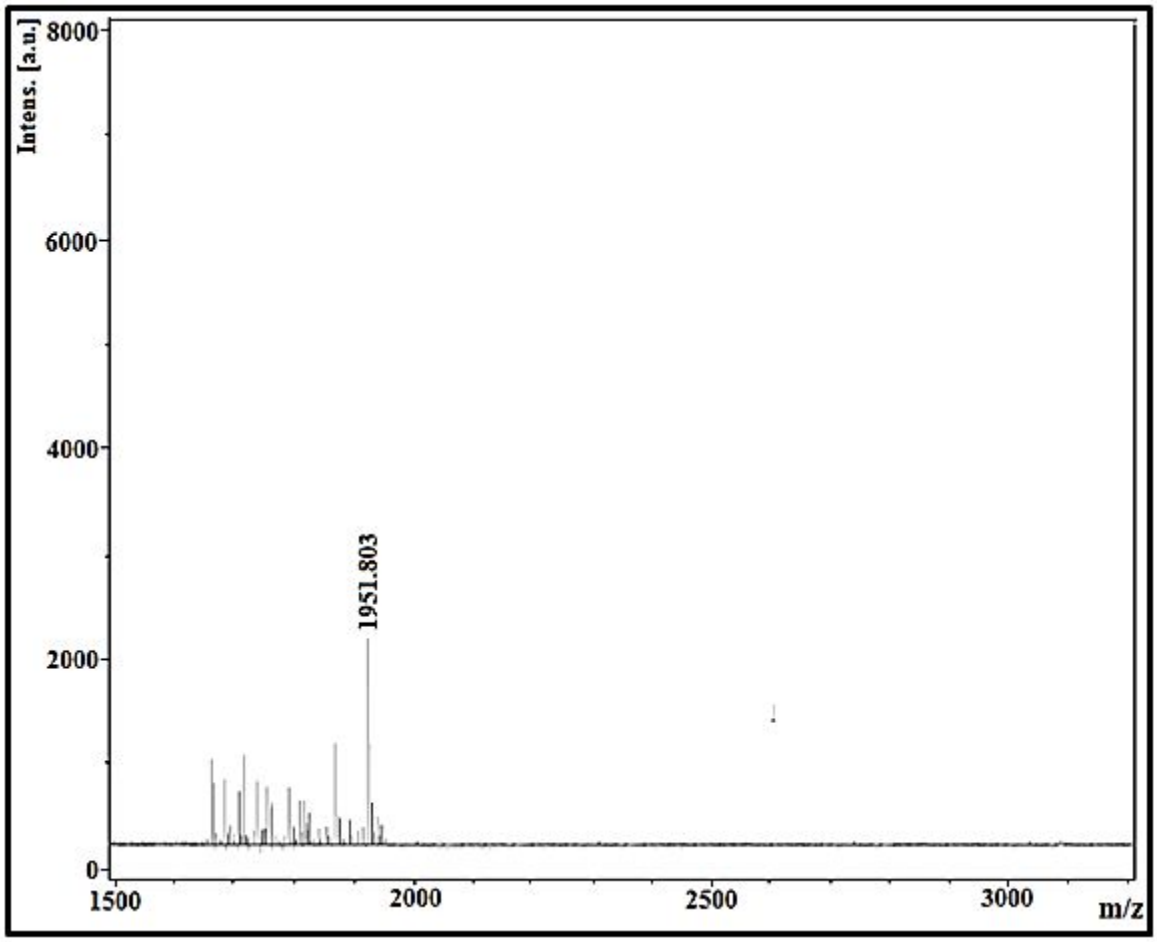

Figure S44. MALDI-TOF mass spectra of compound **10a**

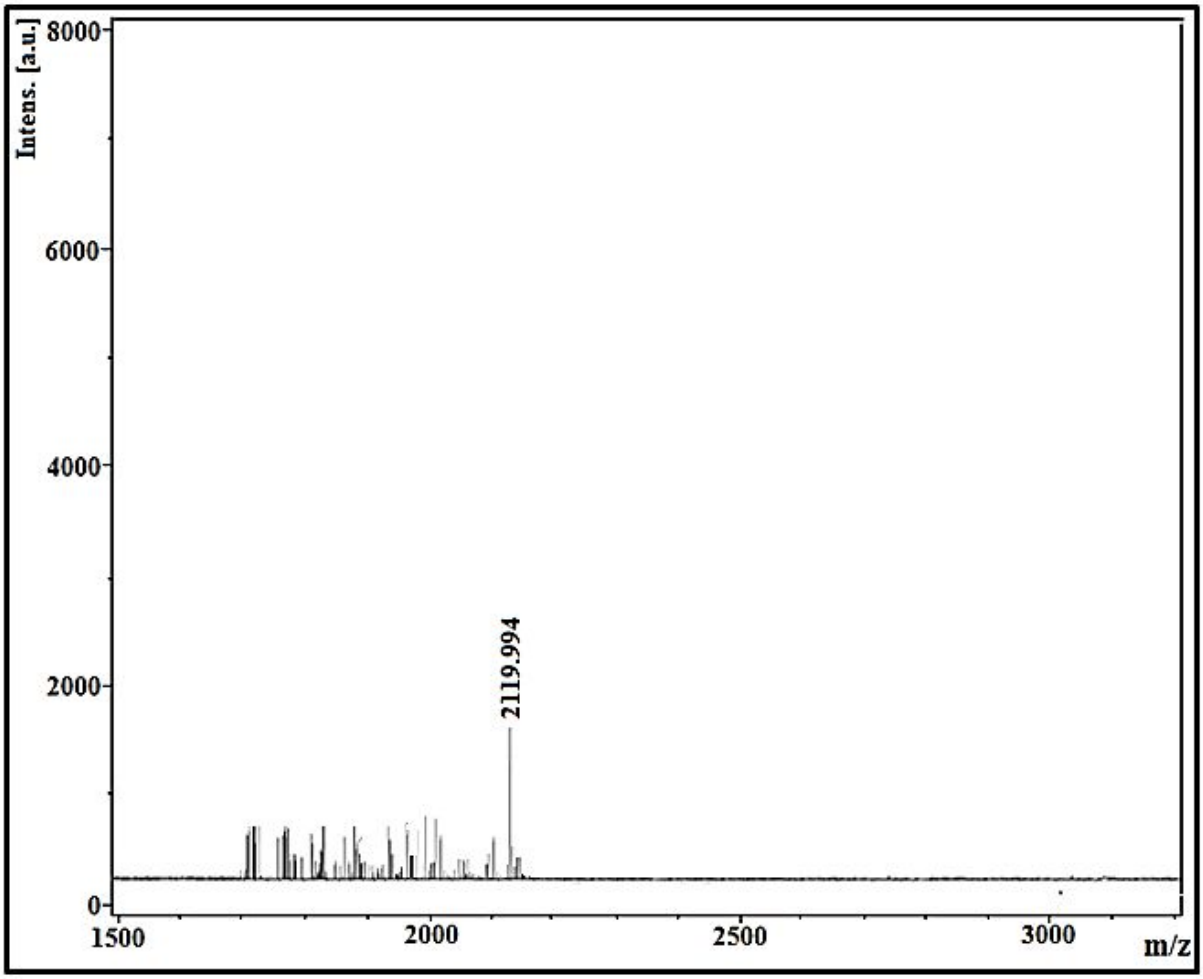

Figure S45. MALDI-TOF mass spectra of compound **10b**

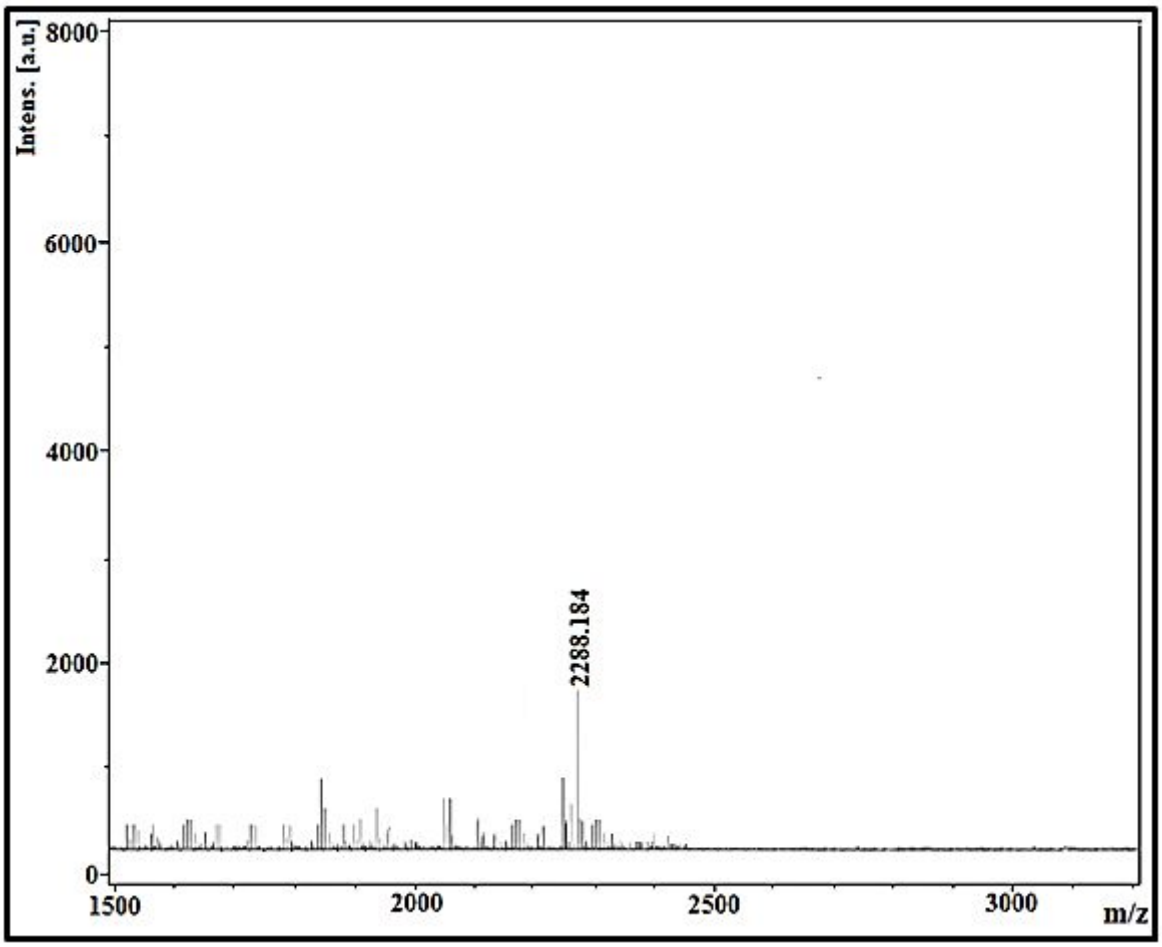

Figure S46. MALDI-TOF mass spectra of compound **10c**

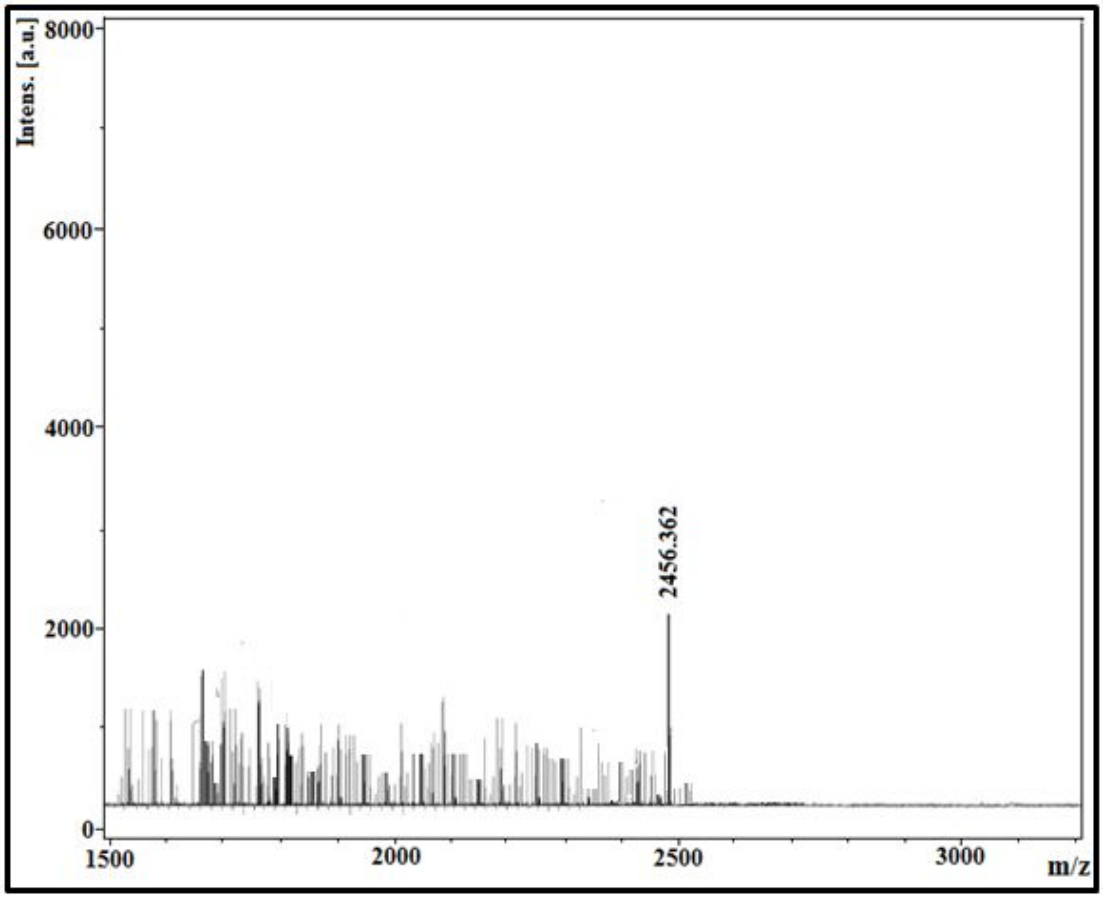

Figure S47. MALDI-TOF mass spectra of compound **10d**

References

1. Pathak, S.K.; Nath, S.; De, J.; Pal, S.K.; Achalkumar, A.S. Contrasting effects of heterocycle substitution and branched tails in the arms of star-shaped molecules. *New J. Chem*. **2017**, *41*, 4680-4688.
2. Tomi, I.H.R.; Al-Heatimi, D.T.A.; Jaffer, H.J. Asymmetric 1,3,4-thiadiazole derivatives: Synthesis, characterization and studying their liquid crystalline properties. *Journal of Molecular Structure*. **2017**, *1141*, 176-185.
3. Sharma, V.S.; Patel, R.B. The effect of position of *tert*-butyl tail group on the formation of liquid crystal in Schiff base ester based homologous series. *Mol.Cryst.Liq.Cryst*. **2017**, 643, 53-65.
4. Kumagai, H.; Hasegawa, M.; Miyanari, S.; Sugawa, Y.; Sato, Y.; Hori,T.; Ueda, S.; Kamiyama, H.; Miyano, S. Facile Synthesis of p-tert-butyl thiacalix[4]arene by the reaction of p-*tert*-butyl phenol with elemental sulphur in the presence of base. *Tetrahedron Letters*. **1997**, 38, 3971-3972.
5. Sharma, V.S.; Sharma, A.S.; Vekariya, R.H. Columnar self-assembly of bowl-shaped luminescent oxadiazole calix[4]arene derivatives. *Journal of Molecular Liquids.* **2018***, 271,* 319-327.